



**POLITECNICO**  
MILANO 1863

Scuola di Ingegneria Industriale e dell'Informazione

Master School in Mechanical Engineering

**The effects of mediolateral vibrations while walking  
on a treadmill: a setup for cognitive task and gait  
analysis**

Supervisor: Prof. Marco TARABINI

Co-Supervisors: Eng. Pietro MARZAROLI

Eng. Stefano MARELLI

Eng. Alex P. MOORHEAD

M.Sc. thesis by

**Martin Grigera Naón**

ID number: 915898

Academic Year 2019/2020



# Table of contents

List of figures.....	3
List of tables.....	5
Abstract.....	6
Chapter 1: Introduction.....	8
1.1 Whole body vibrations.....	8
1.2 Cognitive tasks.....	10
1.3 Devices used to perform vibration tests.....	12
1.3.1 Commercially available shakers.....	13
1.4 Objectives and requirements for this project.....	15
Chapter 2: Design of the machine.....	16
2.1 Selection of the treadmill.....	16
2.2 Vibrating plate.....	17
2.3 Selection of linear rail guides.....	19
2.4 Vertical blades.....	22
2.5 Motor and linear actuator selection.....	24
2.6 Motor-screw flange.....	31
2.7 Lower frame.....	32
2.8 Supporting feet.....	33
2.9 Complete shaker assembly.....	34
2.10 Manufactured machine.....	36
Chapter 3: Modal analysis of the machine.....	37
3.1 FEM methodology.....	37
3.2 Defeaturing and model assumptions.....	37
3.2.1 Treadmill, moving platform, rail carts and linear actuator slider.....	38
3.2.2 Supporting frame, rails, linear actuator body and motor.....	39
3.3 Assembly relations.....	40
3.4 Model settings.....	42

3.5 Effect of standing subject.....	46
3.6 FEM results.....	48
Chapter 4: Preliminary performance analysis of the machine.....	50
4.1.1 Harmonic analysis of the actuated platform.....	50
4.1.2 Set-up for three axis frequency response .....	53
4.2.1 Methodology for the harmonic analysis.....	53
4.3.1 Methodology for the three axis frequency response .....	54
4.3.1 Results and discussion of harmonic analysis .....	55
4.3.2 Results and discussion of the frequency response analysis.....	57
Chapter 5: Cognitive test.....	59
5.1 Testing method and protocol.....	59
5.2 PVT testing device.....	60
5.3 PVT testing prototype.....	62
5.3.1 Method.....	63
5.3.2 Results and discussion.....	63
Chapter 6: Conclusion and future developments.....	67
6.1 Conclusions.....	67
6.2 Further developments.....	67
Bibliography.....	69
Appendix.....	72
[A.1] Data sheet.....	72
[A.2] Draft of the custom parts.....	75
[A.3] Matlab script.....	81

# List of figures

- Figure 1: Sinuous omega shaped path, with pointer placed at the start/stop
- Figure 2: Stroop test: congruent, control and incongruent stimuli
- Figure 3: Team Corporation's shakers: a) Mantis™ b) Cube™ c) Tensor™
- Figure 4: MAST™ 353 at INAIL Research Center, Rome
- Figure 5: Xiaomi WalkingPad A1® treadmill
- Figure 6: COMPOCEL® AL sandwich panel
- Figure 7: CAD drawing of the vibrating plate
- Figure 8: loading directions on the linear rail guide
- Figure 9: model of vibrating plate. a) master rail b) slave rail
- Figure 10: sizing equation of the linear guide from Rollon® catalogue
- Figure 11: Table with admissible load for each linear guide from Rollon®
- Figure 12: scheme of the machine with a) vertical blades b) rail carts c) frame d) treadmill
- Figure 13: Finite element analysis of vertical blade considering misalignment
- Figure 14: buckling analysis of vertical blades
- Figure 15: couples of motors that satisfy the constraints. A) maximum stroke, B) maximum frequency
- Figure 16: Motor Omron® R88M-K1K520T
- Figure 17: Rollon® TV-110 32-32 linear actuator
- Figure 18: motor-screw flange CAD model
- Figure 19: CAD model of the welded aluminum frame
- Figure 20: supporting foot AA model from Vibrostop®
- Figure 21: Vibrating treadmill assembly
- Figure 22: overall dimensions of the vibrating treadmill assembly
- Figure 23: Manufactured vibrating platform
- Figure 24: Lower frame with guides at same height
- Figure 25: combination of multiple parts to moving platform
- Figure 26: combination of multiple parts to supporting frame
- Figure 27: Simplified assembly
- Figure 28: Rail-cart joint
- Figure 29: Definition of the coupling constraint
- Figure 30: Slider-actuator joint (the springs are represented in purple)
- Figure 31: Load diagram of AA 30 feet models (AA 30/R green line)
- Figure 32: model of the feet as springs (on purple)
- Figure 33: Meshing of the supporting frame and vibrating plate
- Figure 34: Scheme of a standing human body
- Figure 35: FEM model of a standing subject
- Figure 36: Location of the accelerometers on the plate
- Figure 37: Nationals Instruments' 9234

Figure 38: Keysight 33210A signal generator  
Figure 39: a) Time domain and b) Power spectra with  $1\text{Hz} \pm 20\text{ mm}$  input  
Figure 40: a) Time domain and b) Power spectra with  $2\text{Hz} \pm 20\text{ mm}$  input  
Figure 41: a) Time domain and b) Power spectra with  $3\text{Hz} \pm 20\text{ mm}$  input  
Figure 42: Total harmonic distortion for all signals  
Figure 43: Representation of the location of the accelerometers  
Figure 44: FRF of the sine wave with  $4\text{ Hz}$  frequency and  $\pm 20\text{ mm}$  amplitude  
Figure 45: Sequence for testing for the different groups  
Figure 46: CANFORD<sup>®</sup> push button  
Figure 47: Arduino<sup>®</sup> WEMOS D1 mini controller  
Figure 48: Case of the WEMOS' housing  
Figure 49: Lid of the WEMOS' housing  
Figure 50: PVT testing prototype  
Figure 51: Subject's 1 average reaction time in each minute  
Figure 52: Subject's 1 average reaction time in each trial  
Figure 53: Average and deviation of the reaction time in each trial

# List of tables

Table 1: Team Corporation shakers comparison

Table 2: Xiaomi WalkingPad A1<sup>®</sup> treadmill specifications

Table 3: mechanical and physical properties of COMPOCEL<sup>®</sup> AL panel

Table 4: loads on each rail cart

Table 5: List of 1S-servo motors produced by Omron<sup>®</sup> considered

Table 6: List of screw linear actuators from Rollon<sup>®</sup> considered

Table 7: Units used in the FEM model

Table 8: Material properties used in the FEM model

Table 9: mass-normalized values of the parameters of the model

Table 10: Vibration modes of vibrating treadmill and standing subject

Table 11: Tests performed for harmonic analysis

Table 12: Tests performed for the frequency response analysis

# Abstract

A lightweight, portable uniaxial shaker, capable of supporting a treadmill and a person on top has been designed and manufactured to measure the influence of medio lateral vibration on the cognitive performance and on the gait parameters of subjects at low excitation frequency (1 Hz) with high amplitude (10 cm).

A FEA of the designed machine to assess the bandwidth of the system up to 46 Hz. The performance analysis of the manufactured shaker measured the acceleration signals on different points of the vibrating plate and assessed the bandwidth of 10 Hz. The selected method and protocol of the cognitive testing was a Psychomotor Vigilance Task (PVT) while walking. A device to run the PVT test has been produced and tested on four subjects. The protocol was validated and the device worked properly and the preliminary acquired data show that there is no influence of a training of fatigue factor when performing a prolonged test.

The machine has been designed and finally tested. Safety protections will be added to test human subjects.





# Chapter 1

## Introduction

People are exposed to whole-body vibrations (WBV) every day when they take a train, a bus or any mean of transportation, also there are jobs that require exposure to vibrations over a prolonged period of time. This can affect the physical health and safety of people, as well as the brain capacity. To help understand and evaluate the potential detrimental effects of vibration exposure, various cognitive tests can be used which measure reaction time and reasoning ability. Since there are few studies evaluating the effects of medio-lateral WBV compared to the effects of vertical WBV, this thesis will focus on medio-lateral vibrations. To test the human response to vibrations in the lab, different types of shakers are used to simulate a vibrating environment. This thesis will also examine the requirements of designing and building a machine suitable for producing medio-lateral WBV as well as a device for performing different cognitive tests.

### 1.1 Whole body vibrations

Whole-body vibration refers to mechanical oscillations that are transmitted to the human body through contact with a vibrating interface such as the floor or seat of a moving vehicle, or through the vibrations of a power tool. People are exposed to these vibrations every day during transportation and some are also exposed to vibrations for extended periods of time during work such as crane and heavy equipment operators, truck drivers, aircraft pilots, train conductors and other transportation workers. About 26% of Italian workers are exposed to potentially harmful mechanical vibrations in their workplace [1]. While some studies have shown potentially beneficial effects of WBV in sports under controlled and limited exposure [2] [3], extended exposure to WBV without control over amplitude or frequency is considered an occupational hazard which may be detrimental to

the employee's health. Detrimental effects can range from annoyance and discomfort on sedentary activities [4] to lasting harmful damage caused by resonance with various organs [cit.?].

The standard ISO 2631-1:1997 [5] gives the guidelines for measuring the vibration exposure to WBV by measuring the acceleration signal between the vibrating surface and the human body. The calculation of the vibration exposure also depends on the direction and position of the human body (standing, seated or recumbent). Accordingly, the standard determines thresholds, commonly referred to as Exposure Action Value (EAV) above which the employers are required to take action to control and reduce exposure and an Exposure Limit Value (ELV) not to be exceeded because it represents a high risk for the person.

Many studies done on workers exposed to WBV have shown a correlation between WBV exposure and low back pain (LBP) and musculoskeletal disorders (MSDs) [31] [6] [7]. According to the European Agency for Safety and Health at Work (EU-OSHA) [8], MSDs account for 38.1% of occupational diseases in the European Union (EU). Bovenzi [9] conducted a study on professional drivers who were initially unaffected by LBP and after a two-year follow-up, the cumulative incidence of LBP was around 38% with some of them having high pain intensity and severe disability. Birlik [10] measured the exposure to WBV in suburban and intercity train drivers and found that the daily exposure exceeded the ISO-recommended EAV safety limit and were therefore at risk of developing spinal disorders. Ghi Chan Kim et al. [11] found that helicopter pilots were significantly more prevalent to have degenerative changes in the cervical spine than military clerical workers. Both groups, pilots and clerical workers had similar office working conditions, the only difference was that pilots had more flight hours where they were exposed to WBV.

Since there are many field studies which prove the exposure of WBV during work, laboratory studies were initiated to understand their effects, both in standing and seated subjects. Results by Shibata [12] showed that subject discomfort level increased with increasing levels of acceleration and that standing people are more sensitive to vertical vibration than seated people. By varying the direction (fore-aft, medio-lateral and vertical

WBV) and the acceleration (0.2; 0.4; 0.8 m/s<sup>2</sup> r.m.s.) produced by shakers, Shibata also demonstrated that the direction of the oscillations has a great influence on the subject's response. Subashi et al. [13] showed that the different standing postures have a significant role on the apparent mass when evaluating the human response to WBV.

In order to test the influence of oscillation on walking subjects, several studies [14] [15] used a treadmill connected to a vertically oscillating platform while a motion capture system acquired the kinematic data. This proves that the method of having a vibrating treadmill is a good way to expose a walking person to WBV in a lab environment.

McAndrew et al. [36] found out that the gait parameters of a subject walking are most influenced when exposed to medio-lateral vibrations. Studies by Sari et al. [37] and Hak et al. [38] both tested how lateral perturbations of the walking surface affects the stability of a person. Most of the studies done to walking subjects under vibrations focused on the kinematic response only and almost none studied how the cognitive performance is affected.

## **1.2 Cognitive tasks**

Cognitive tasks are used to assess the mental capability of a subject and the way it processes information. They are a good way to determine the brain capacity and possible damage or impairment. Nasreddine et al. [23] demonstrated that cognitive tasks can be used to evaluate subjects with Alzheimer's disease and mild cognitive impairment that are more likely to suffer from dementia.

Current literature [24] [25] has shown that WBV may reduce the mental capacity of a subject and the effects can be compared to sleep deprivation, alcohol intoxication or certain mental diseases. Costa et al. [25] tested drivers' cognitive performance using the 'omega test' which is designed to examine the precision in the handling of mechanisms and careful attention of subjects. It consists of two knobs that move a pointer along a sinuous line, and it should be done without touching the edge (Figure 1). This was performed inside a van, under three different conditions, van halted, van performing a

circuit in asphalt (mean acceleration RMS of  $0.2\text{m/s}^2$ ) and on cobblestone (mean acceleration RMS of  $0.54\text{m/s}^2$ ). Statistical significant difference was found between the subjects performance under the WBV profiles (van moving on asphalt and cobblestone), where all the parameters of performance (Number of errors, total error duration and total time taken) were worse with the increasing vibration exposure. The parameters of the vibration were not precisely controlled, since driving in different surfaces is not a precise way to control the vibration signal. In our tests we will have a precise control on the vibration signal and also use tasks that only evaluates the cognitive capacity, not taking into account the motor capacity.

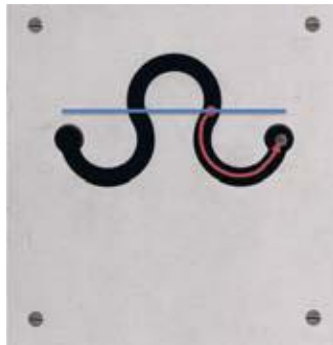


**Figure 1: Sinuous omega shaped path, with pointer placed at the start/stop**

Exposure to WBV also correlates to longer reaction times to both audible and visual stimuli and may also disrupt the ability to sustain attention [26] [27]. A common task that measures the speed in which subjects respond to a visual, audible, or tactile stimulus is the psychomotor vigilance test (PVT), also known as reaction time test. It is a simple task in which the subject must respond to a simple auditory, visual, or mechanical stimulus. This task is commonly used to test sleep depravity, fatigue, and alertness in people [16] [17]. Azizan et al.[28] found that the exposure to WBV on seated subjects promotes drowsiness, this was done by using a PVT test prior and after exposure.

Another common task used to test cognitive performance is the Stroop test that measures the delay of reaction time between congruent and incongruent stimuli. The Stroop test is used to measure selective attention capacity as well as processing speed ability and executive processing skills such as decision making and managing real-world interference

[18]. This test was used to observe the effects of WBV on attention [29] and on the mental condition [30] of participants.

The test consists of a written list of colors where each word has a different color ink. First the participants need to read the written color names of the words independently of the color of the ink (for example, if the word “blue” was written in red ink they would have to read "blue"). In a second experiment, participants were required to say the ink-color of the letters independently of the written word. A congruent stimulus is when the word and the word color refer to the same color and an incongruent stimulus is when the word and the ink color differ (Figure 2).

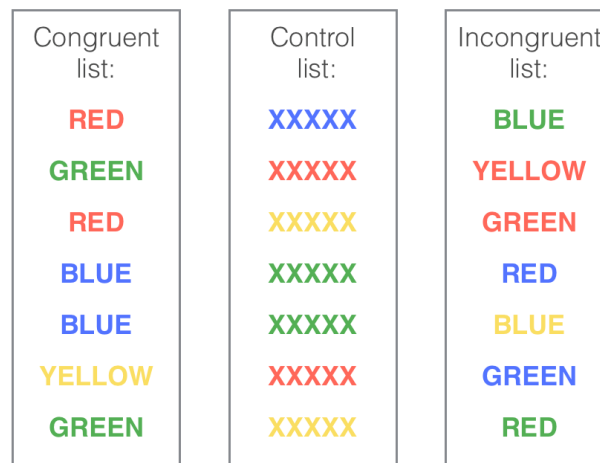


**Figure 2: Stroop test: congruent, control and incongruent stimuli**

### 1.3 Devices used to perform vibration tests

To impose medio-lateral vibrations to a walking subject, a machine capable of generating a controlled mechanical oscillation is needed. These machines can be classified in monoaxial or multiaxial shakers, depending on the number of vibrating axis. The monoaxial or linear shakers generate vibrations in only one axis, and they tend to be simpler and smaller machines. Multiaxial shakers are used if a multiaxial response is needed since the simultaneous effect of triaxial vibration is different from the sum of the effects of subsequent uniaxial excitations.

The shakers can be also be classified by the actuating system that produces the oscillations on the end-effector [19]. Two big families exist: hydraulic shakers and electrodynamic shakers. The hydraulic shakers are characterized by the hydraulic actuation of the platform of the shaker; they are controlled by a servo-valve, where the input is a voltage signal generated by a frequency generator, and according to the value and sign of the voltage signal the piston of the actuator moves upwards or downwards. The electrodynamic shakers are actuated by an electromagnetic force created by a motor that has a frequency generator that sends a signal to a current amplifier. This force drives the armature of the shaker along the field coils, which are large electromagnets.

Both types of shakers are complimentary since for the most part hydraulic shakers have longer displacement but cannot respond as fast to control frequencies. While, in general, electrodynamic shakers can respond quickly to frequency but have more limited displacement.

### 1.3.1 Commercially available shakers

A general performance comparison of shakers produced by Team Corporation is reported in Table 1. The shakers are also shown in Figure 3.

<b>Performance</b>	<b>Mantis™</b>	<b>Cube™</b>	<b>Tensor™</b>	<b>Electro-dynamic systems</b>
<b>Degrees of freedom</b>	6	6	6	6
<b>Frequency bandwidth</b>	100Hz	250Hz	700Hz	2000Hz
<b>Displacement peak-peak</b>	150mm	100mm vert. 50mm hor.	13mm	Shaker dependent
<b>Typical payload</b>	50-2000 Kg	25-500 Kg	5-50 Kg	Shaker dependent
<b>Max. force rating</b>	315 KN	62 KN	36 KN	Shaker dependent

**Table 1: Team Corporation shakers comparison**

The values of force rating, stroke and payload are related to the increasing size of shakers. Greater and heavier structures involve a narrower frequency bandwidth that prevents the use of a shaker in a range of testing fields [20].



**Figure 3: Team Corporation's shakers: a) Mantis™ b) Cube™ c) Tensor™**

Since electrodynamic shakers tend to be more compact, cost-effective, and require less maintenance while providing a greater frequency bandwidth than hydraulic shakers, they are typically preferred in the industrial sector. In the research environment hydraulic shakers are preferred because of their higher precision. An example of a hydraulic shaker used in a research laboratory for academic purposes, especially in the health and safety at work (HSW) field, is the MAST™ 353, shown in Figure 4 owned by the Istituto nazionale Assicurazione Infortuni sul Lavoro (INAIL) Research Center, located in Rome. This shaker can have a maximum payload of 680 Kg to be applied on a round table of 2 meters radius and covers an excitation range of 0.1 to 100 Hz.



**Figure 4: MAST™ 353 at INAIL Research Center, Rome**



Not all laboratories are able to have this kind of structure because it requires a lot of space and also because, the optimal position of the shaker would be embedded in the ground, to avoid undesirable vibrations thus needing a meter dig on the floor.

#### **1.4 Objectives and requirements for this project**

The objective of this thesis is to design a machine capable of supporting the weight of a person of 100 kg and the treadmill while producing medio-lateral vibrations. It needs to be portable, lightweight, and occupy as little space as possible since it should be also placed in a motion capture laboratory for gait analysis [21] [22]. Then the study focuses on the design of the device used for the cognitive testing.

In this thesis, first the design of each component and the selection of the different parts is showed to understand the final design of the machine, then a FEM modal analysis is explained. After that, a preliminary performance analysis of the manufactured machine is presented and the method for the cognitive testing and the device used is presented. Finally, there is the conclusions and discussion of possible further developments on this study.

## Chapter 2

### Design of the machine

To measure the effect of medio-lateral vibrations on walking subjects it is necessary to have a machine that can safely support the weight of a person, 100 kg or lower, while performing consistently and delivering accurate and reliable results. The overall aim of the shaker is to produce random and low frequency vibrations, from 0 to 10 Hz, and be able to produce large strokes of up to  $\pm 100$  mm in the lower frequency ranges to reproduce the medio-lateral vibrations people are subjected in different means of transport. In this chapter the design, component specifications, construction and testing of the medio-lateral vibrating treadmill will be described to demonstrate how these requirements were met.

#### 2.1 Selection of the treadmill

The selection of the treadmill was the first and most important step because the size and weight of the treadmill directly influences the size of the whole machine. Since the goal was to design a lightweight and easily movable machine, the treadmill should be as small and light as possible. Furthermore, the testing is done to walking subjects so a treadmill achieving walking speeds of 5 km/h was enough. Taking all this into account, the selected treadmill was the Xiaomi WalkingPad A1® (Xiaomi Běijīng, China) (figure 5), since it is small, light (28 Kg is very light for a treadmill) and can achieve speeds of 6 km/h. The specifications of the treadmill are showed on table 2, considering that the size and weight are lower than other commercially available options.



**Figure 5: Xiaomi WalkingPad A1® treadmill**

Lowest Speed	0,5 km/h
Maximum Speed	6 km/h
Maximum load	100 kg
Product weight	28 kg
Dimensions	143 x 55 x 13 cm

**Table 2: Xiaomi WalkingPad A1® treadmill specifications**

The benefits of this treadmill are that it is light, small and has a simple geometry since it does not have a dashboard and bars that add weight, instead it is controlled remotely.

## **2.2 Vibrating plate**

Being that the vibrating plate is the supporting surface of the treadmill and will be the primary moving part of the machine, it is important that it has low inertia, because the

lower the weight, the higher the payload of the shaker. It should also have high stiffness to have a high first natural frequency so that the machine does not go into resonance in the low frequency operation range. Since the dimensions of this plate need to be bigger than the treadmill to support it, having a solid aluminum plate would be too heavy. In order to reduce weight while maintaining a high stiffness, the plate was made with a 20 mm thick COMPOCEL<sup>®</sup> AL (Castenaso, Italy) that is a sandwich panel with a core in aluminum honeycomb bonded to two skins of aluminum, greatly reducing the weight while maintaining a high stiffness, this is showed in figure 6. The physical and mechanical properties of the panel are presented on table 3.

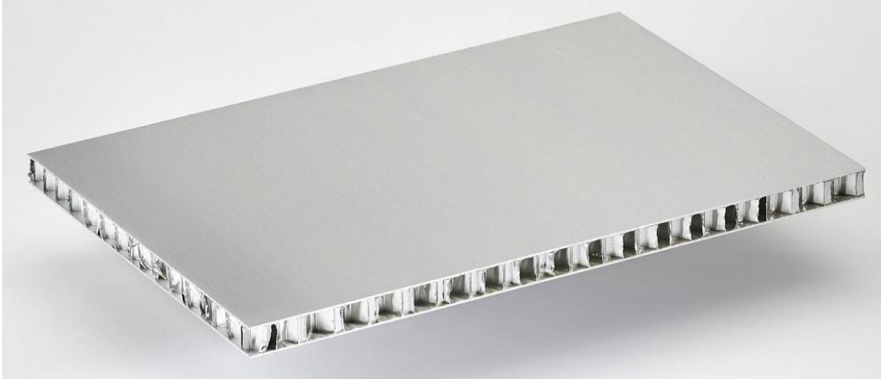


**Figure 6: COMPOCEL<sup>®</sup> AL sandwich panel**

Thickness	20 mm
Skin thickness	1 mm + 1 mm
Panel weight	7.3 kg/m <sup>2</sup>
Maximum load	1350 N
Elastic modulus	68000-70000 MPa

**Table 3: mechanical and physical properties of COMPOCEL<sup>®</sup> AL panel**

Figure 7 shows the CAD drawing of the upper side of the plate together with its overall dimensions. A total of eight through holes a1) allow the connection of the vibrating

plate and the slider of the linear actuator. The through holes pattern b1) allow the connection of the plate to the four carts of the linear rail guides.

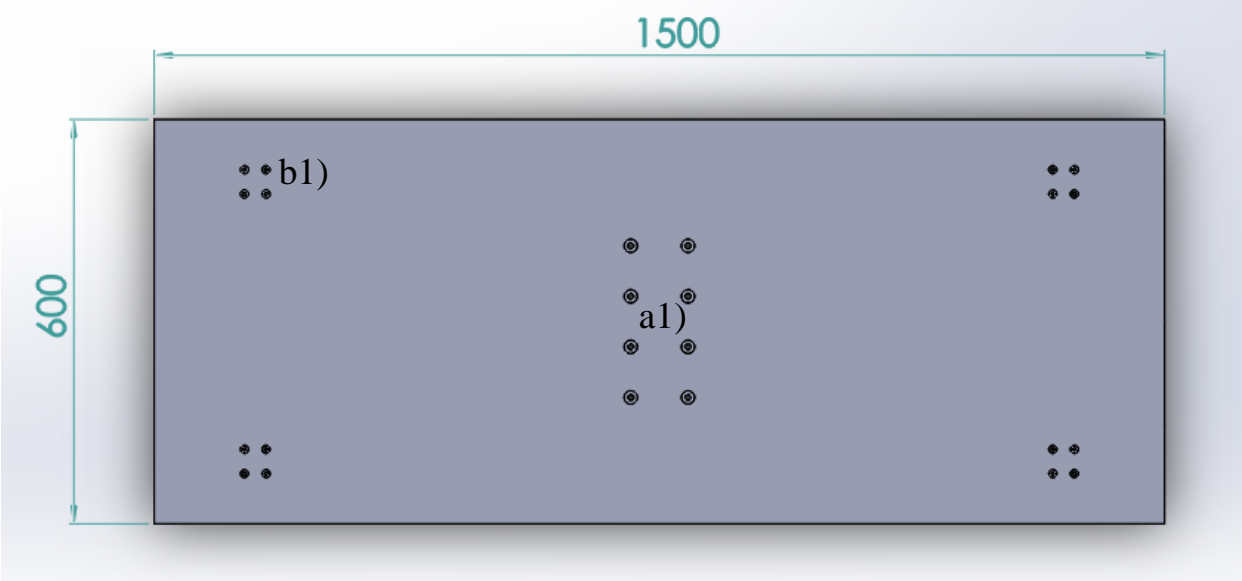


Figure 7: CAD drawing of the vibrating plate

### 2.3 Selection of linear rail guides

The first step to select the linear rail guides from the Rollon® (Vimercate, Italy) was to make a static assessment to know which were the loading requirements of the guides. A calculation of the loads in the different directions with respect to the rail was needed. In Figure 8, the different directions are represented.

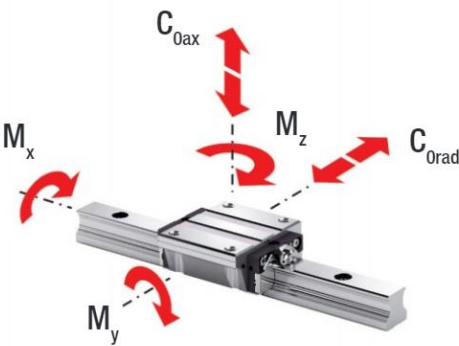
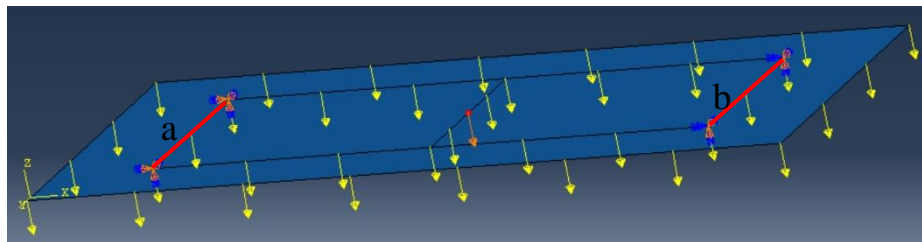


Figure 8: loading directions on the linear rail guide

To do this, the vibrating plate was modelled as a shell element with a body force representing its weight ( $3.65e^{-7} \text{ kg/mm}^3 \times 9.81 \text{ m/s}^2 = 3.58e^{-6} \text{ N/mm}^3$ ) and a concentrated load in the middle point of the plate representing the weight of the subject and the treadmill ( $(100\text{kg} + 28\text{kg}) \times 9.81\text{m/s}^2 = 1255 \text{ N}$ ). The boundary conditions were modelled at the places where the carts would be joined to the plate, and one rail was considered the master rail and was fixed in all directions and the other the slave meaning the lateral displacement was left free while it was fixed in all the other directions. Figure 9 represents the model of the plate with its boundary conditions.



**Figure 9: model of vibrating plate. a) master rail b) slave rail**

After the simulation, the values of  $M_x$ ,  $M_y$  and  $F_z$  on all the rail carts were obtained and are showed on table 4.

<b><math>M_x</math> [Nm]</b>	<b><math>M_y</math> [Nm]</b>	<b><math>F_z</math> [N]</b>
<b>-78</b>	<b>-7,1</b>	<b>340,7</b>
<b>-76,4</b>	<b>7,2</b>	<b>342,8</b>
<b>77,5</b>	<b>7,1</b>	<b>338,3</b>
<b>76</b>	<b>-7,9</b>	<b>343,8</b>

**Table 4: loads on each rail cart**

The sizing of the linear guide was done using the equation (Figure 10) from the Rollon® catalogue, considering a safety factor of 2.5 suggested for applications with large amount of vibrations.

$$\frac{P_{Orad}}{C_{Orad}} + \frac{P_{Oax}}{C_{Oax}} + \frac{M_1}{M_x} + \frac{M_2}{M_y} + \frac{M_3}{M_z} \leq \frac{1}{S_0}$$

$P_{Orad}$  = carico radiale applicato (N)  
 $C_{Orad}$  = carico radiale ammissibile (N)  
 $P_{Oax}$  = carico assiale applicato (N)  
 $C_{Oax}$  = carico assiale ammissibile (N)  
 $M_1, M_2, M_3$  = momenti esterni (Nm)  
 $M_x, M_y, M_z$  = momenti massimi ammissibili nelle diverse direzioni di carico (Nm)

**Figure 10: sizing equation of the linear guide from Rollon® catalogue**

The values of the admissible loads were obtained from the catalogue (figure 11) and finally the rail guide MRS20 was chosen with a length of 880 mm, enough to have the desired  $\pm 10$  cm stroke amplitude.

Tipo	Capacità di carico [N]		Momenti statici [Nm]		
	C din.	C <sub>Orad</sub> stat. C <sub>Oax</sub> stat.	M <sub>x</sub>	M <sub>y</sub>	M <sub>z</sub>
MRS15 MRS15W MRT15W	8500	13500	100	68	68
MRT15SW	5200	6800	51	18	18
MRS20 MRS20W MRT20W	14000	24000	240	146	146
MRT20SW	9500	14000	70	49	49
MRS20L MRS20LW	16500	30000	300	238	238
MRS25 MRS25W MRT25W	19500	32000	368	228	228
MRT25SW	12500	17500	175	69	69
MRS25L MRS25LW	26000	46000	529	455	455
MRS30 MRS30W MRT30W	28500	48000	672	432	432
MRT30SW	17500	24000	336	116	116
MRS30L MRS30LW	36000	64000	896	754	754
MRS35 MRS35W MRT35W	38500	62000	1054	620	620
MRT35SW	25000	36500	621	209	209
MRS35L MRS35LW	48000	83000	1411	1098	1098
MRS45 MRS45W MRT45W	65000	105000	2363	1378	1378
MRS45L MRS45LW	77000	130000	2925	2109	2109

Tab. 1

**Figure 11: Table with admissible load for each linear guide from Rollon®**

When using two linear rails in parallel, it is very important to guarantee this parallelism between them to prevent the jamming of the carts. Since we were considering they are going to be supported on a welded frame, and they are going to be separated 1200mm from each other, this parallelism constraint would not be met. In order to prevent this problem, we consider having two vertical plates 2 mm thick on each of the carts located on the slave rail, allowing a small lateral displacement in case the parallelism tolerances are not met. A basic scheme of this design is showed in figure 12.

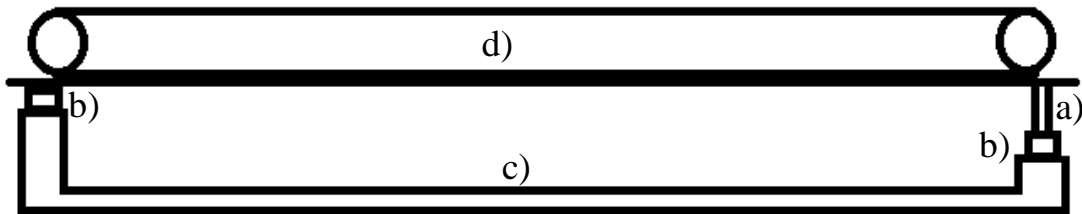


**Figure 12: scheme of the machine with a) vertical blades b) rail carts c) frame d) treadmill**

## 2.4 Vertical blades

The vertical blades are thin plates made of aluminum of 50 mm high, 48 mm width (length of the rail carts) and 2 mm thick. The function is to allow a small lateral displacement in case the rails are not aligned perfectly to prevent the jamming of the rail carts. To test this, a static general finite element analysis was done using ABAQUS considering a 0.5 mm misalignment of the rails. The plate was modelled with quad shell elements with an approximate size of 1 mm. The blade was completely fixed on the upper side, while a displacement of 0.5 mm perpendicular to the shell was applied on the bottom. The simulation results can be seen on figure 13.



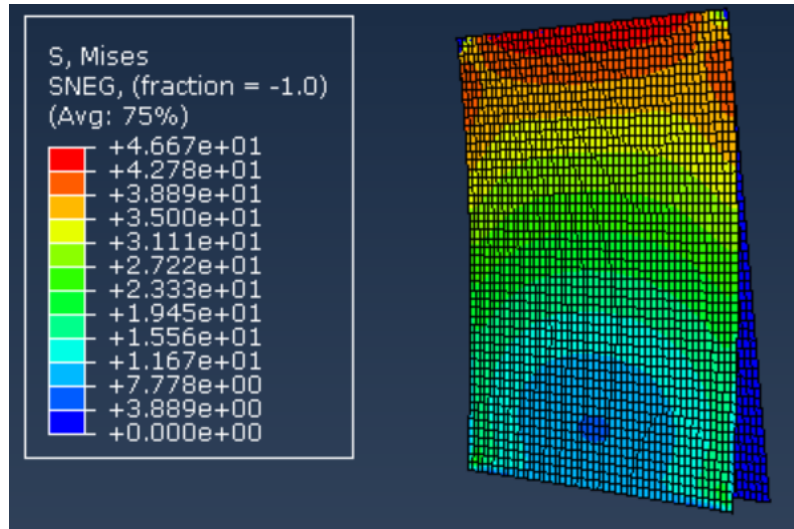


**Figure 13: Finite element analysis of vertical blade considering misalignment**

From this simulation the maximum stress obtained due to misalignment would be 46.67 MPa, much lower than the yield strength of any aluminum alloy.

The possibility of buckling was also analyzed by fixing the bottom part of the plate while applying a uniform compressive load on top. This was done in a buckle simulation step on ABAQUS. The results obtained are showed on the figure 14.

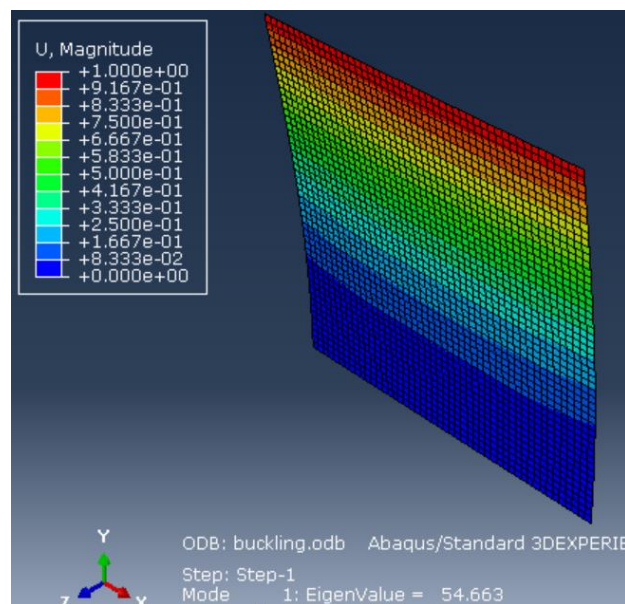


**Figure 14: buckling analysis of vertical blades**

To calculate the load needed for buckling we need to multiply the EigenValue obtained from the analysis time the length of the applied load (54,663N/mm x 48 mm = 2623,8 N). Since the maximum compressive force present on the rail carts when the person is on the treadmill is 343.8 N, much lower than 2623.8 N then buckling would not occur.

## 2.5 Motor and linear actuator selection

To minimize backlash and maximize stiffness only actuators with recirculating ball screws were considered. Screw and motor combinations had to be considered simultaneously since both contribute to the dynamics of the system and the couple of motor-screw is bounded by constraints that depend on parameters of the motor such as its moment of inertia ( $J_M$ ) and on the reducer, the screw pitch ( $\tau$ ) and its moment of inertia ( $J_T$ ). We need to get possible combinations of screw and motor that satisfy the requests. The process of selection was done following the procedure explained by Giberti et al. [32]

According to Giberti et al. the best performance of the system is achieved when the inertia of the load referred to the motor shaft coincided with the inertia of the motor, where there is a power balance of the system. To determine the motor and screw combination two conditions were evaluated, one were the strokes of the linear actuator are maximum (100 mm amplitude with a frequency of 1.125 Hz), and the other condition were the frequency is the maximum requested (10 Hz with a stroke amplitude of 1.25 mm).

The functioning of the machine can be described as a balancing of power:

$$\frac{T_M}{\tau} - F_L = \left( \frac{J_M}{\tau^2} + M_L \right) a_L \quad [eq. 1]$$

In our case  $T_M$  is the torque of the motor,  $\tau$  is the pitch of the screw,  $F_L$  is the linear force in the slider of the screw,  $M_L$  is the mass of the moving load (mass of the cart plus vibrating plate, plus treadmill and medio-lateral apparent mass of a standing person exposed to low frequency, considered as 0.4 of the actual mass according to the study of

Tarabini et al. [33]),  $a_L$  is the acceleration of the moving load and  $J_m$  is the moment of inertia of the motor.

By integrating this equation for the cycle time and rearranging the terms, we get an equation that calculates the square of the nominal torque for the task requested. Obtaining:

$$T_{M,rms}^2 = \int \left( \tau^2 F_L^{*2} + J_M^2 \frac{a_L^2}{\tau^2} + 2J_M F_L^* a_L \right) \frac{dt}{t_a}$$

$$T_{M,rms}^2 = \tau^2 F_{L,rms}^{*2} + J_M^2 \frac{a_{L,rms}^2}{\tau^2} + 2J_M (F_L^* a_L)_{mean} \quad [eq 2]$$

With  $F_L^* = F_L + M_L a_L$ . The square of the nominal torque of the motor ( $T_{M,N}^2$ ) must be greater than the mean square of the torque required by the motor ( $T_{M,rms}^2$ ). Obtaining:

$$T_{M,N}^2 \geq T_{M,rms}^2 = \tau^2 F_{L,rms}^{*2} + J_M^2 \frac{a_{L,rms}^2}{\tau^2} + 2J_M (F_L^* a_L)_{mean}$$

By ordering terms, we get to an expression that separates the contribution of the motor, the task and the screw.

$$\frac{T_{M,N}^2}{J_M} \geq 2[(F_L^* a_L)_{mean} + F_{L,rms}^* a_{L,rms}] + \left( \frac{\tau}{\sqrt{J_M}} F_{L,rms}^* - \frac{\sqrt{J_M}}{\tau} a_{L,rms} \right)^2 \quad [eq 3]$$

$$\alpha = \frac{T_{M,N}^2}{J_M} \quad \beta = 2[(F_L^* a_L)_{mean} + F_{L,rms}^* a_{L,rms}]$$

The term  $\alpha$  depends only on the motor and the term  $\beta$  depends only on the task because it includes the resistant forces and the load acceleration.

By solving the inequality as function of  $\tau$  two values are obtained. These are the maximum and minimum value of the pitch  $\tau$  for a given motor showed on equation 5. Another constraint on the pitch of the screw is the minimum one to guarantee the maximum

load speed. Having  $v_{L,max}$  as the maximum load speed and  $\omega_{M,max}$  the maximum rotation speed of the motor.

$$\tau \geq \frac{v_{L,max}}{\omega_{M,max}} \quad [eq\ 4]$$

$$\tau_{min}, \tau_{max} = \sqrt{J_M} \frac{\sqrt{\alpha - \beta + 4a_{L,rms}F_{L,rms}^*} \pm \sqrt{\alpha - \beta}}{2F_{L,rms}^*} \quad [eq\ 5]$$

These constraints on the pitch of the screw are calculated for each motor considering the ones from the catalogue of the 1S servo motors and Accurax G5 from Omron® (Kyoto, Japan) (showed in table 5). The possible linear actuators considered are from the precision line from Rollon® in particular the TH, TT and TV series (showed in table 6). Highlighted in green are the final selection of motor and screw.

Motor Name	Rated torque [Nm]	Rated speed [rpm]	Peak torque [Nm]	Max speed [rpm]	Moment of inertia [kgm <sup>2</sup> *10 <sup>-4</sup> ]
R88M-1M10030T-230V	0.318	3000	1.11	6000	0.0968
R88M-1M20030T-230V	0.637	3000	2.2	6000	0.2832
R88M-1M40030T-230V	1.27	3000	4.5	6000	0.5052
R88M-1M75030T-230V	2.39	3000	8.4	6000	2.0742
R88M-1L1K030T-230V	3.18	3000	9.55	6000	2.5542
R88M-1L1K530T-230V	4.77	3000	14.3	6000	2.5542
R88M-1L75030C-400V	2.39	3000	7.16	5000	1.7542
R88M-1L1K030C-400V	3.18	3000	9.55	5000	2.5542
R88M-1L1K530C-400V	4.77	3000	14.3	5000	2.5542
R88M-1L2K030C-400V	6.37	3000	19.1	5000	2.8542
R88M-1L3K030C-400V	9.55	3000	28.7	5000	7.3122
R88M-1M1K020T-230V	4.77	2000	14.3	3000	6.5042
R88M-1M1K520T-230V	7.16	2000	21.5	3000	9.5042
R88M-K1K520T-230V	7.16	2000	21.5	3000	7.99
R88M-1M40020C-400V	1.91	2000	5.73	3000	2.8472

<b>R88M-1M60020C-400V</b>	2.86	2000	8.59	3000	4.2472
<b>R88M-1M1K020C-400V</b>	4.77	2000	14.3	3000	6.5042
<b>R88M-1M1K520C-400V</b>	7.16	2000	21.5	3000	9.5042
<b>R88M-1M2K020C-400V</b>	9.55	2000	28.7	3000	12.7042
<b>R88M-1M3K020C-400V</b>	14.3	2000	43	3000	17.4122
<b>R88M-1M90010T-230V</b>	8.59	1000	19.3	2000	9.5042
<b>R88M-1M90010C-400V</b>	8.59	1000	19.3	2000	9.5042
<b>R88M-1M2K010C-400V</b>	19.1	1000	47.7	2000	45.1122
<b>R88M-1M3K010C-400V</b>	28.7	1000	71.7	2000	73.1122

**Table 5: List of 1S-servo motors produced by Omron® considered**

<b>Linear actuator Name</b>	<b>Pitch [mm]</b>	<b>Axial load capacity [N]</b>	<b>Maximum velocity [m/s]</b>	<b>Critical velocity [m/s]</b>
<b>TH-90 12-05 SP2</b>	5	4300	0.56	0.6975
<b>TH-90 12-10 SP2</b>	10	3600	1.11	1.3950
<b>TH-90 12-05 SP4</b>	5	4300	0.56	0.6975
<b>TH-90 12-10 SP4</b>	10	3600	1.11	1.3950
<b>TH-110 16-05 SP2</b>	5	12640	0.42	1.6489
<b>TH-110 16-10 SP2</b>	10	9900	0.83	3.5041
<b>TH-110 16-16 SP2</b>	16	9900	1.33	5.7995
<b>TH-110 16-05 SP4</b>	5	12640	0.42	1.6489
<b>TH-110 16-10 SP4</b>	10	9900	0.83	3.5041
<b>TH-110 16-16 SP4</b>	16	9900	1.33	5.7995
<b>TH-145 20-05 SP2</b>	5	14700	0.33	2.3897
<b>TH-145 20-20 SP2</b>	20	12250	1.33	9.5453
<b>TH-145 25-10 SP2</b>	10	16270	0.53	5.9348
<b>TH-145 20-05 SP4</b>	5	14700	0.33	2.3897
<b>TH-145 20-20 SP4</b>	20	12250	1.33	9.5453
<b>TH-145 25-10 SP4</b>	10	16270	0.53	5.9348
<b>TT-100 12-05</b>	5	6600	0.5	0.2786

<b>TT-100 12-10</b>	10	6600	1	0.5572
<b>TT-155 16-05</b>	5	12300	0.5	0.6987
<b>TT-155 16-10</b>	10	9600	1	1.3931
<b>TT-155 20-05</b>	5	14300	0.5	0.9130
<b>TT-155 20-20</b>	20	13300	2	3.6093
<b>TT-225 20-05</b>	5	14300	0.5	0.9130
<b>TT-225 20-20</b>	20	13300	2	3.6093
<b>TT-225 25-05</b>	5	15900	0.5	1.1831
<b>TT-225 25-10</b>	10	15700	1	2.3662
<b>TT-225 25-25</b>	25	14700	2.5	5.7782
<b>TT-310 32-05</b>	5	21600	0.4	1.5346
<b>TT-310 32-10</b>	10	31700	0.8	3.0134
<b>TT-310 32-32</b>	32	19500	2.5	9.6447
<b>TV-80 20-05</b>	5	14300	0.5	1.1520
<b>TV-80 20-20</b>	20	13300	2	4.5538
<b>TV-110 32-05</b>	5	21600	0.4	1.6736
<b>TV-110 32-10</b>	10	31700	0.8	3.2865
<b>TV-110 32-32</b>	32	19500	2.5	10.3083
<b>TV-140 20-05</b>	5	14300	0.5	1.6435
<b>TV-140 20-20</b>	20	13300	2	6.4969
<b>TV-140 25-05</b>	5	15900	0.5	2.1296
<b>TV-140 25-25</b>	25	14700	2.5	10.4012

**Table 6: List of screw linear actuators from Rollon® considered**

Additional constraints for the selection of the motor and screw pair to guarantee its functioning are:

- Maximum torque required by the motor
- Maximum linear and critical speed of the linear actuator
- Maximum forces on the slider (loads have to be lower than the load capacity of the screw)

- Maximum engine rpm

These calculations have been done with a MATLAB® code for the two operating conditions required, maximum stroke amplitude and maximum frequency. Obtaining possible combinations of motors and linear screws. In figure 15 is possible to see which pairs satisfy the constraints mentioned for both operating conditions, where the motors are indicated in the horizontal axis and the screws on the vertical one, the dots represent a possible pair that satisfies all the constraints. The script used is on the Appendix.

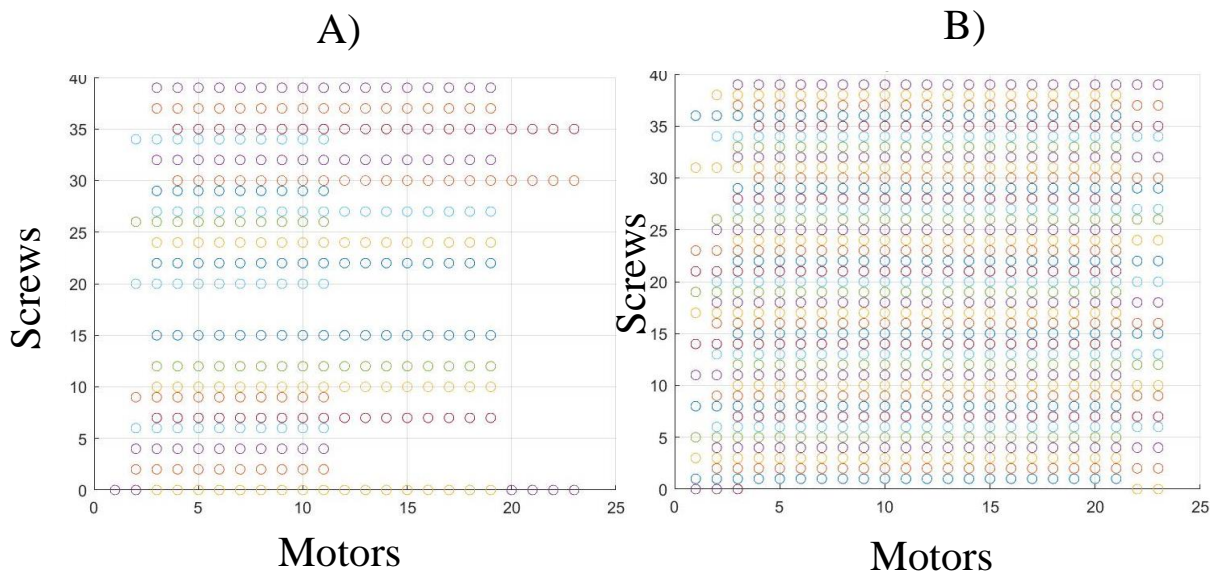


**Figure 15: couples of motors that satisfy the constraints. A) maximum stroke, B) maximum frequency**

The final motor selection was the R88M-K1K520T of 230 V (number 14 on figure 15) because, even though the lab can support the use of motors of 400 V, the machine is designed to be movable and to be used in different environments where a 230 V outlets are more common (showed in figure 16) (data sheet presented in the appendix).



**Figure 16: Motor Omron® R88M-K1K520T**

The linear guide chosen in combination with the motor was the TV-110 32-32 (number 35 from figure 15), having the highest pitch available (32 mm) we can obtain high speeds. The guide TT-310 32-32 was another guide with 32 mm pitch, but was discarded because it is much bigger and costly (310 mm of transversal dimension versus the 110 mm of the TV-110) (showed in figure 17) (data sheet presented in the appendix).



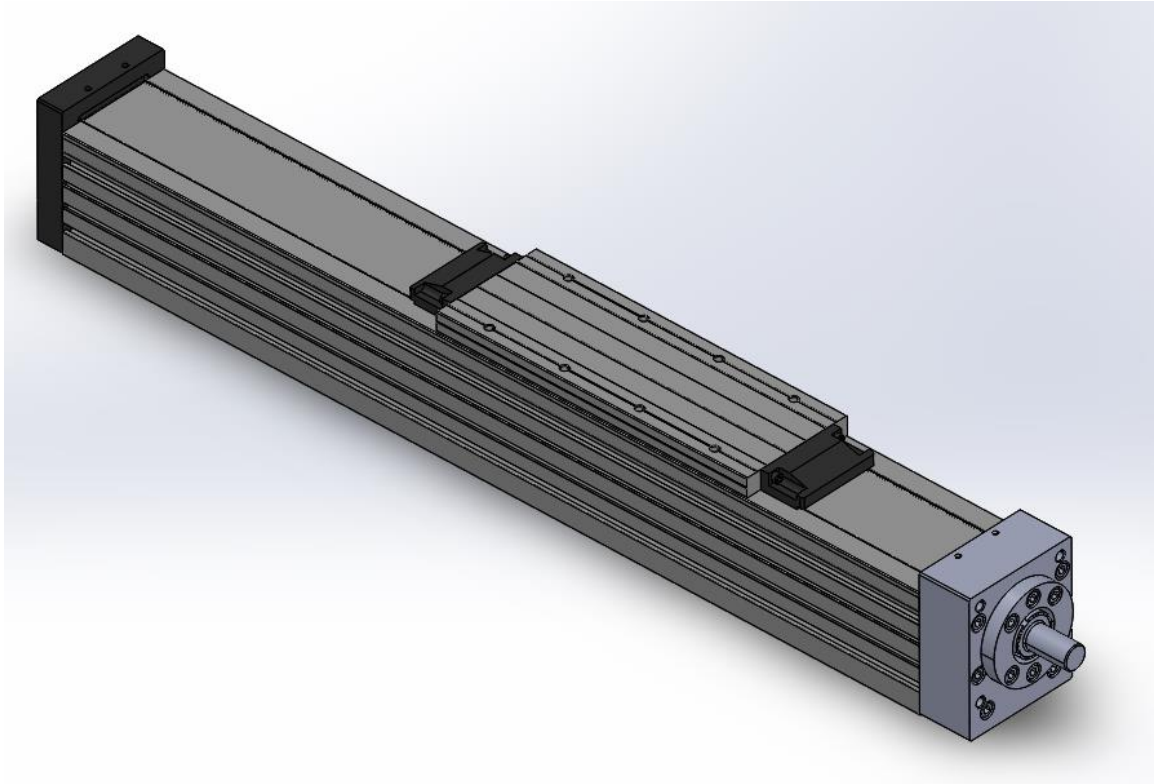


**Figure 17: Rollon® TV-110 32-32 linear actuator**

## **2.6 Motor-screw flange**

The motor-screw flange is the element that supports the motor and connects it to the linear actuator. It encloses the coupling of the motor shaft to the linear actuator shaft, so it needs to be open, in order to tighten the screws of the flexible joint.

Figure 18 shows the CAD model of the flange. The hole a2) allows the space for the shafts of the motor and screw and the flexible joint between them. The M8 threaded holes pattern b2) allow the connection of the motor. The through holes c2) allow the connection with the screw assembly using four M10 bolts.

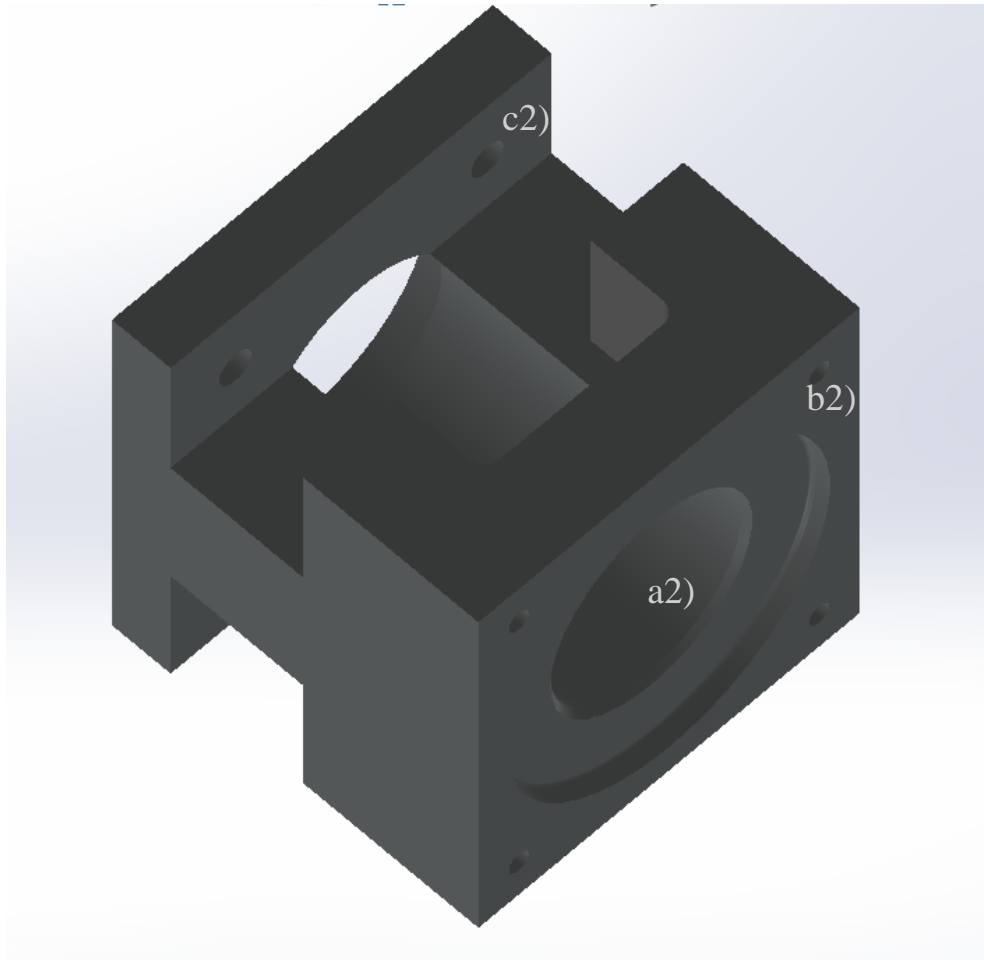


**Figure 18: motor-screw flange CAD model**

## **2.7 Lower frame**

The lower frame is the part that acts as a base and supports the rails of the linear guides and the screw assembly, it is a non-moving part and must be fixed to the ground. Since this is a big part it is very important to save on material to lower weight and costs, therefore it was designed as a welded aluminum frame, instead of using a solid base. The frame is made with hollow rectangular profiles welded together, allowing the support of the components while saving weight due to the hollow profiles.

Figure 19 shows a CAD model of the welded frame. The 10 through holes pattern a3) are used to connect the frame with the linear screw assembly using M6 bolts. The 14 holes b3) on each side are used to connect the rails of the linear guides using M5 bolts. The height of these two sides are different because as it was explained in the paragraph 2.3, the design was made considering that the parallelism of the two rails cannot be guaranteed with the manufacturing process. To solve this problem, the carts of one rail would have the vertical blades, to allow a small displacement, this is why one rail needs to be lower than the other. The 8 through holes pattern c3) are used to connect the feet that support the frame. The holes d3) are used to attach possible railings to the machine for safety, so the subjects have something to hold to while the machine is working.

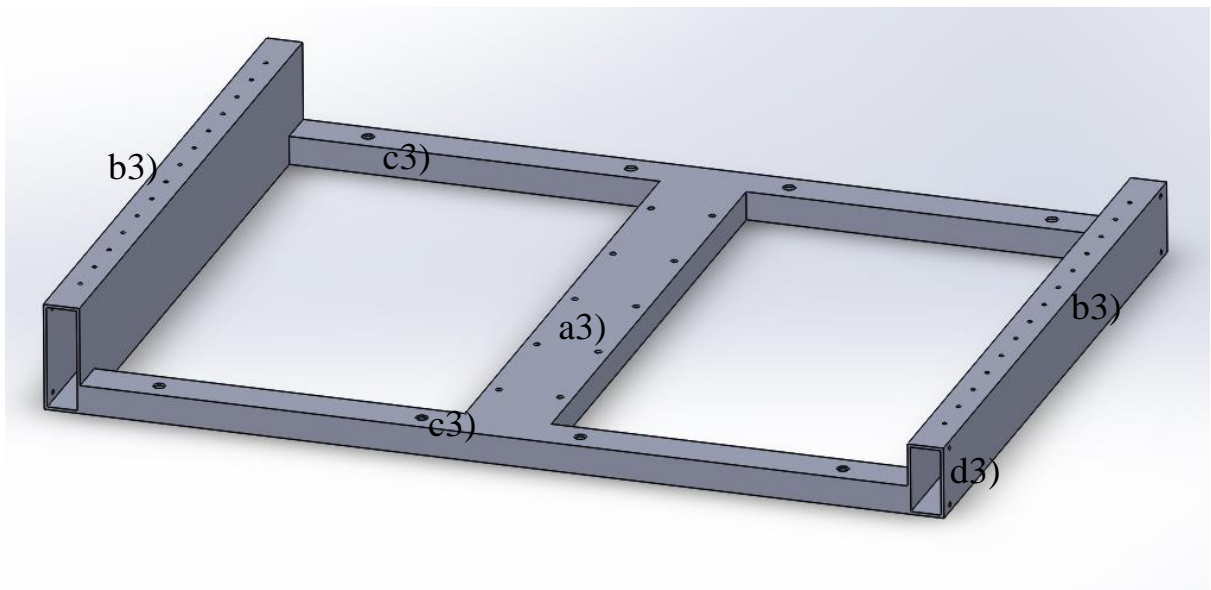


**Figure 19: CAD model of the welded aluminum frame**

## **2.8 Supporting feet**

The supporting feet chosen were the AA30/R from Vibrostop® (Milan, Italy) (showed in figure 20) because they have a load capacity of 50-100 daN, which is enough to support the machine with a person on top. Furthermore, the height of these feet is 36 mm, which was the smallest option, this reduces the height of the whole machine and it is beneficial

for the safety of the person that is going to be walking on top of it. Another benefit from these kinds of feet is that they can be bolted to the ground to increase the stiffness and prevent the machine from sliding.



**Figure 20: supporting foot AA model from Vibrostop®**

## **2.9 Complete shaker assembly**

The complete assembly is shown in figure 21 and its overall dimension are shown in figure 22.

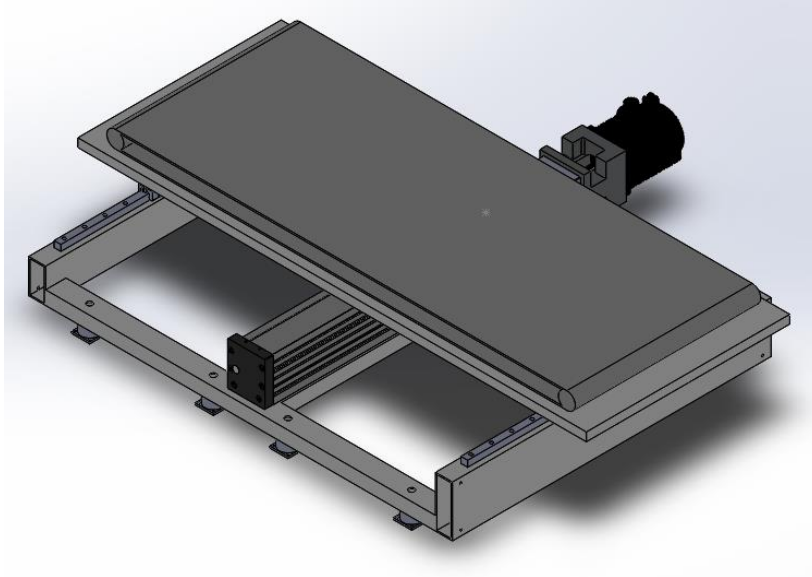


**Figure 21: Vibrating treadmill assembly**

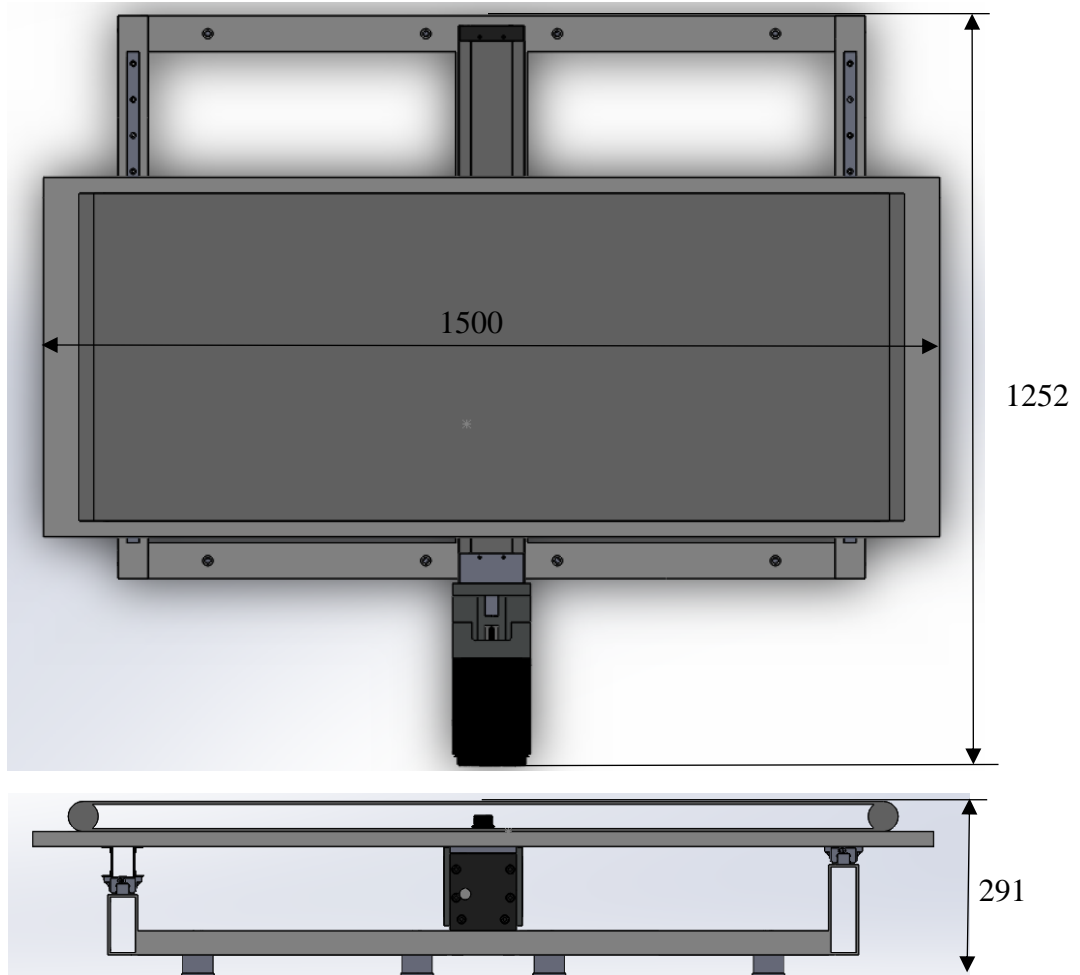


**Figure 22: overall dimensions of the vibrating treadmill assembly**

## 2.10 Manufactured machine

In figure 23 a picture of the manufactured vibrating platform without the treadmill is showed.

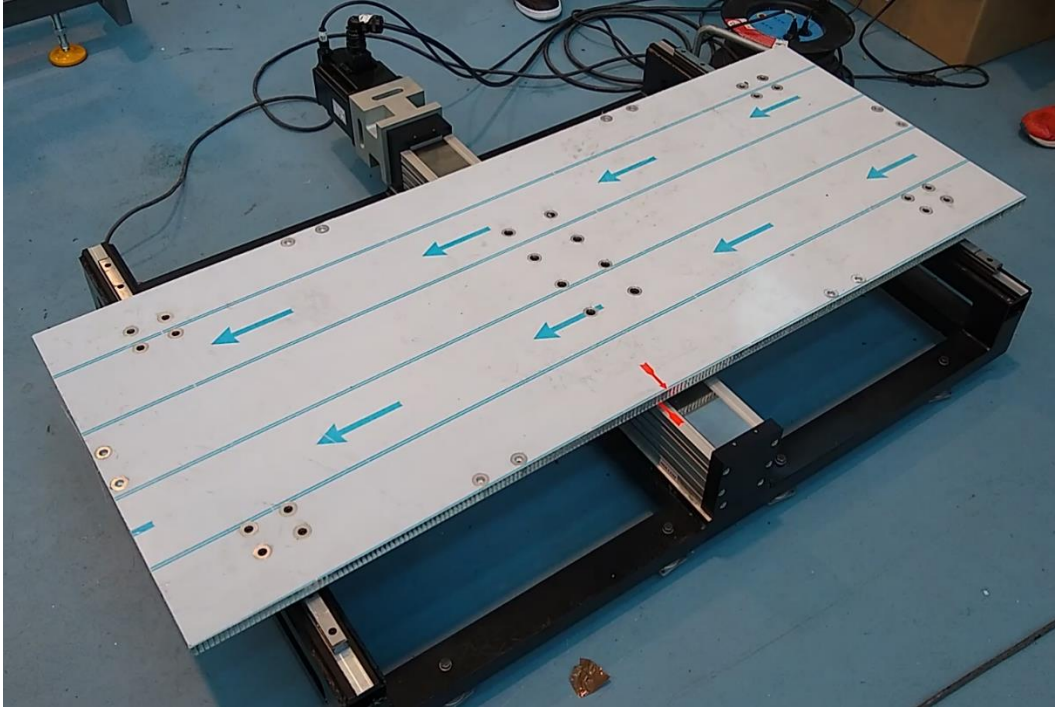


**Figure 23: Manufactured vibrating platform**

An important change in the final design of the machine is that the two parallel rails of the linear guides are on the same height as it can be seen in figure 24, and the vertical blades will not be needed since the manufacturers could produce the frame with the tight tolerances requested for the planarity and parallelism of the rails.

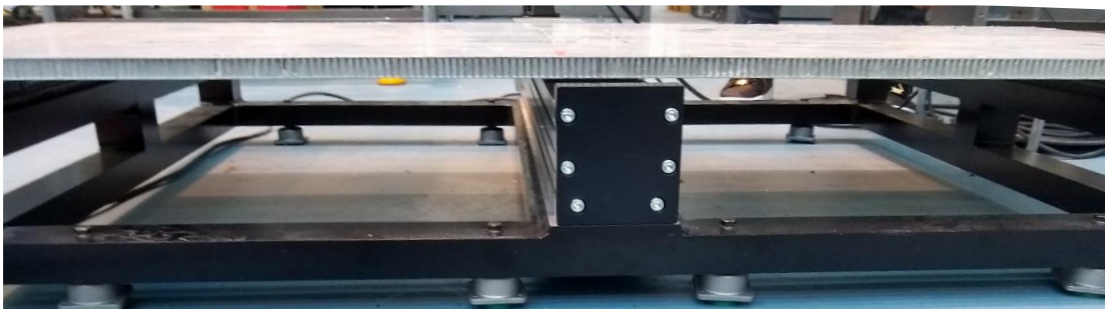


**Figure 24: Lower frame with guides at same height**

## Chapter 3

### Modal analysis of the machine

In this chapter a Finite Element Model (FEM) of the vibrating treadmill is performed in order to make a modal analysis. The natural frequencies and the mode shapes of the machine will be obtained, particularly focusing on the lower vibration modes that will give us the bandwidth of frequencies for the machine. The effect of a standing subject on the treadmill will also be taken into account.

#### 3.1 FEM methodology

Modelling of the vibrating treadmill is used to predict how a physical object will behave under certain boundary conditions. In order to perform a finite element modelling an exact representation of the machine is not needed, instead a simplification of the structure without losing the mechanical meaning of the components is done. This, speeds up the computational process during the FEM simulation.

The modal analysis using FEM is used to determine the natural frequencies and mode shapes of a structure. The analysis gives the eigenvalues and eigenvectors of the problem that represent the natural frequency and their mode shape. For our case, only the first few modes are of interest because the goal is to obtain a bandwidth much higher than the frequencies the treadmill is going to be subjected to.

#### 3.2 Defeating and model assumptions

Some simplification to the real system is needed in order to simulate on the computer complex systems in real life. These simplifications or assumptions lets us obtain the information of the behavior of the system with a certain degree of accuracy and conformity with the experimental results with a reduced computational workload.

This section shows the simplifications and assumptions made for the components of the 3D model. The parts are based on the CAD parts with certain modifications and simplifications required by the FEM practices. Many small features are removed in the FEM parts and certain parts that in the CAD model are separated, in the FEM are joined together becoming a single part.

### 3.2.1 Treadmill, moving platform, rail carts and linear actuator slider

Since the treadmill will be completely fixed to the moving platform made of COMPOCEL<sup>®</sup> aluminum they can be modelled as one part. The same happens with the rail carts and the linear actuator slider that will be bolted to the moving platform in such a way that the upper surface of the carts and slider will be completely fixed to the lower surface of the platform, therefore they can be modelled as one part in the FEM analysis. In this FEM analysis the vertical blades on one of the linear guides was also taken into account. This part is showed in figure 25.

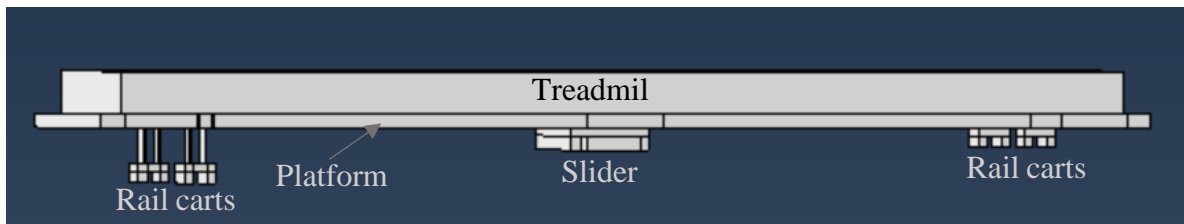


**Figure 25: combination of multiple parts to moving platform**

In this model some simplifications in the shape of the rail carts has been done in order to facilitate the meshing procedure and all the fillets and small holes used for bolting the pieces have been removed to further improve the meshing procedure, without changing the structural properties of the whole part.

Also, the platform and the treadmill has been modelled as solid bodies, assigning the equivalent material properties such as the density value that fits the real mass value.



Finally, geometrical partitions have been done to the part to allow the assignment of different materials properties to different regions and to have a structured or sweep mesh.

### 3.2.2 Supporting frame, rails, linear actuator body and motor

All the remaining parts are modelled as one body since the rails and the linear actuator body are bolted to the supporting frame and the motor is bolted to the flange that is bolted to the linear actuator body, and all this joints have perfect surface contact. This part is showed in figure 26.

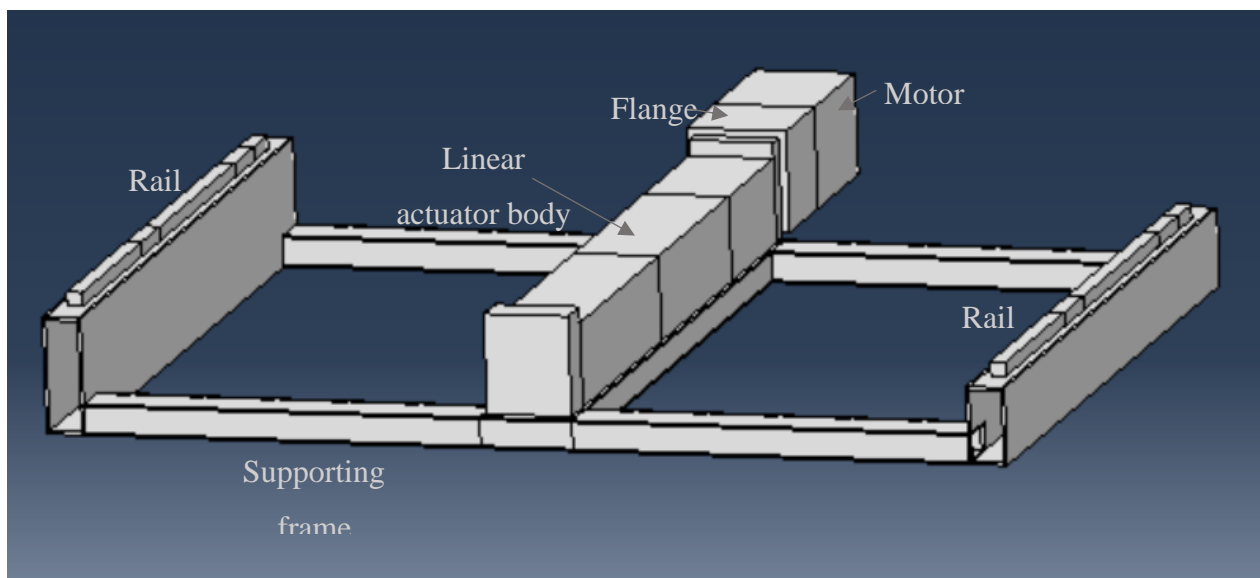


**Figure 26: combination of multiple parts to supporting frame**

In this part as well, the shapes of the pieces have been simplified, the small holes used for bolting have been eliminated. The shape of the body of the linear actuator, the flange and the motor have been modelled as rectangular shaped prisms to facilitate the meshing procedure.

Finally, the geometrical partitions have been done to have a structured or sweep mesh and to assign different material properties to different regions as well as to facilitate the assembly and the coupling relations with the moving platform part.

### 3.3 Assembly relations

The parts have been assembled in the assembly module on Abaqus and the results are showed in figure 27.

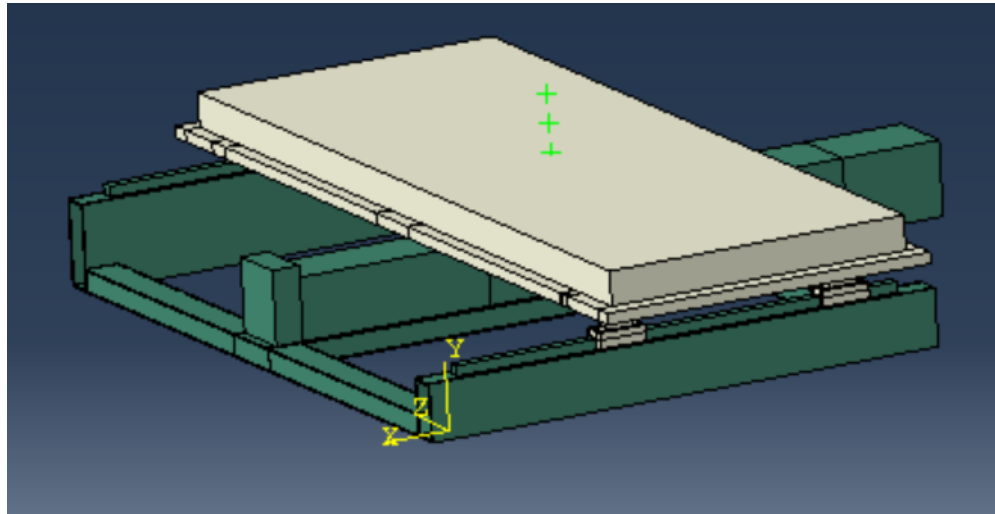


**Figure 27: Simplified assembly**

The next step is to model the different relations in the joint of the rails with the carts and the joint between the linear actuator body and the slider, otherwise the structure would be over constrained and would give misleading results.

The joint of the four carts and rails should allow the translation of the carts in the longitudinal direction of the rail while blocking the movement in all the other directions. In figure 28 this joint is presented.

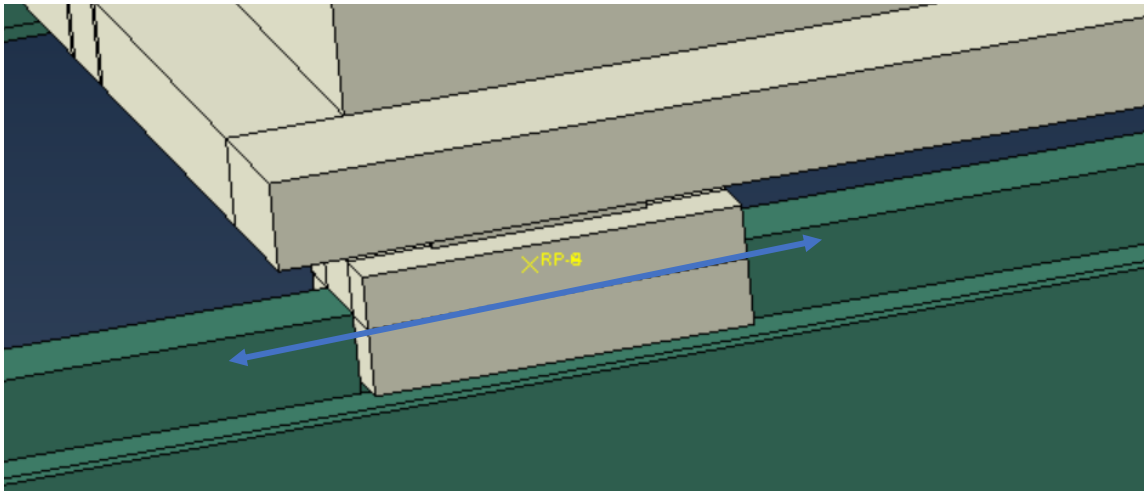


**Figure 28: Rail-cart joint**

To perform these relative constraints between the parts in Abaqus we need to apply a kinematic coupling in the interaction module between each cart and each rail. To do this first a reference point is defined on the bottom surface of each cart and on the top surface of the rails. Then the reference point of the carts is coupled with the inner surface of the cart and the reference point on the rails is coupled with the surface of the rails, in both cases constraining all degrees of freedom (DOF). This ties the motion of the selected nodes to a rigid body motion defined by the reference point. To allow the relative translation of the carts another kinematic coupling is defined between the two reference points allowing just the translation in the longitudinal direction of the rail, while constraining all the other DOF. The definition of the coupling constraint is showed in figure 29.

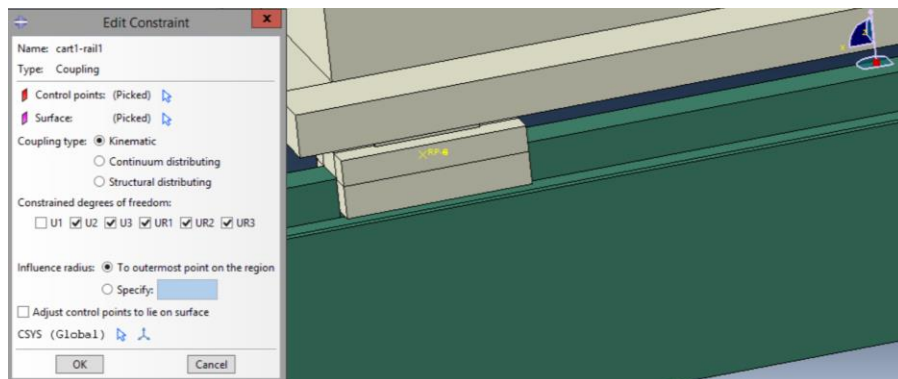


**Figure 29: Definition of the coupling constraint**

The joint between the slider and the linear actuator body should allow small rotations along the longitudinal axis of the slider because the linear ball screw actuator is not rigid in terms of rotations, there is a compliance that is modelled as one spring in each corner of the slider connected to the linear actuator body with a stiffness of 5500N/mm, as it was done in P. Marzaoli's thesis [34]. In figure 30 the joint is illustrated.

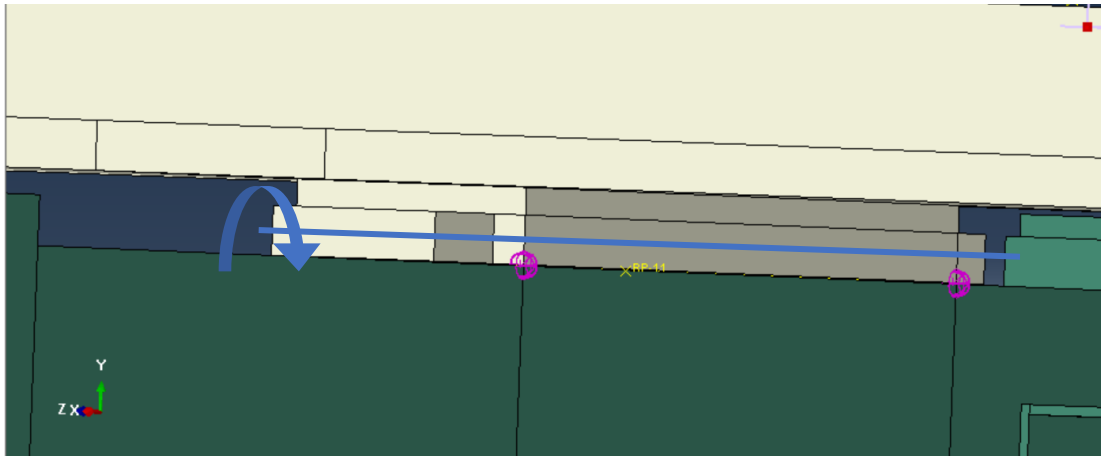


**Figure 30: Slider-actuator joint (the springs are represented in purple)**

To allow the relative rotation another kinematic coupling is needed where a reference point defined on the slider is coupled with the nodes on the lower surface of the slider and another reference point defined in the linear actuator is coupled with the nodes on the upper surface of the actuator, and in both cases all DOF are constraint. Then another coupling is done between the two points allowing just the rotation in the axis of the slider while constraining all the other DOF.

### **3.4 Model settings**

To set up the model for the FEM analysis we need to give different material properties to the parts, considering the proper units of measure. The units used in the model are shown in table 7.

<b>Quantity</b>	<b>FEM model</b>
Length	mm
Force	N
Mass	Ton ( $10^3$ Kg)
Time	S
Stress	MPa
Density	Ton/mm <sup>3</sup>
Stiffness	N/mm

**Table 7: Units used in the FEM model**

The materials used in the model are steel for the linear guides and rails, aluminum for the supporting frame, the flange and the slider of the linear actuator. Then some material properties were added to parts such as the motor, the treadmill and linear actuator body that do not correspond to a real material, but a density was given in relation to their weight in relation to their volume. For the COMPCEL<sup>®</sup> AL supporting plate the properties were given according to the manufacturer's data sheet presented in the appendix. The values of the material properties are showed in table 8.

<b>Material/Component</b>	<b>Density [ton/mm<sup>3</sup>]</b>	<b>Young Modulus [MPa]</b>	<b>Poisson ratio</b>
<b>Steel</b>	$7.8 \times 10^{-9}$	206000	0.3
<b>Aluminum</b>	$2.7 \times 10^{-9}$	69000	0.33
<b>Motor</b>	$3.47 \times 10^{-9}$	206000	0.3
<b>Treadmill</b>	$5.96 \times 10^{-10}$	69000	0.33
<b>Linear actuator body</b>	$2.17 \times 10^{-9}$	69000	0.33
<b>Compocel plate</b>	$3.65 \times 10^{-10}$	69000	0.33

**Table 8: Material properties used in the FEM model**

Then, a frequency analysis is defined in the step module of Abaqus, where the first ten modes are requested as an output. Regarding the fixing of the structure in real life it will be supported by eight AA30/R feet from Vibrostop® that are made with rubber inside. These feet are modelled as springs using the suggested stiffness value from the load diagram given by the manufacturer. Giving a stiffness of approximately 1600 N/mm. The load diagram for the AA/30R feet is showed in figure 31.

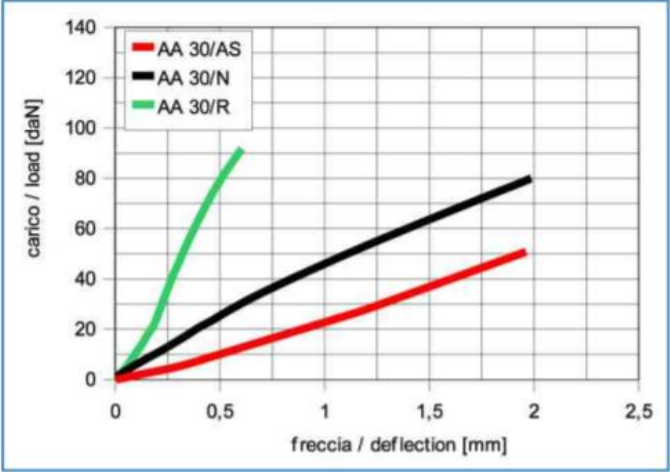


**Figure 31: Load diagram of AA 30 feet models (AA 30/R green line)**

In the FEM model the springs connect the bottom of the frame where the feet would be located to the ground, as it can be seen on figure 32.

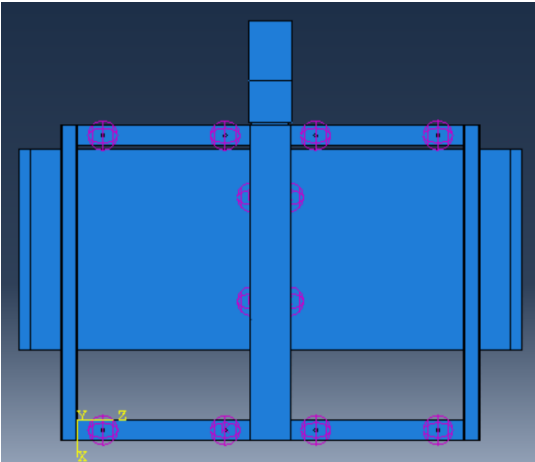


**Figure 32: model of the feet as springs (on purple)**

Finally, in the mesh module the parts have been meshed using linear Hex elements with full integration method. The parts have been portioned to have structure and sweep mesh types. The size of the elements was selected to avoid elements too deformed. With an element size of 15 mm approximately on the whole assembly expect for the thickness of the vibrating plate and the rail carts of the linear guides that have a size of 8 mm approximately there is a convergence to a result. The mesh of the parts is showed in figure 33.

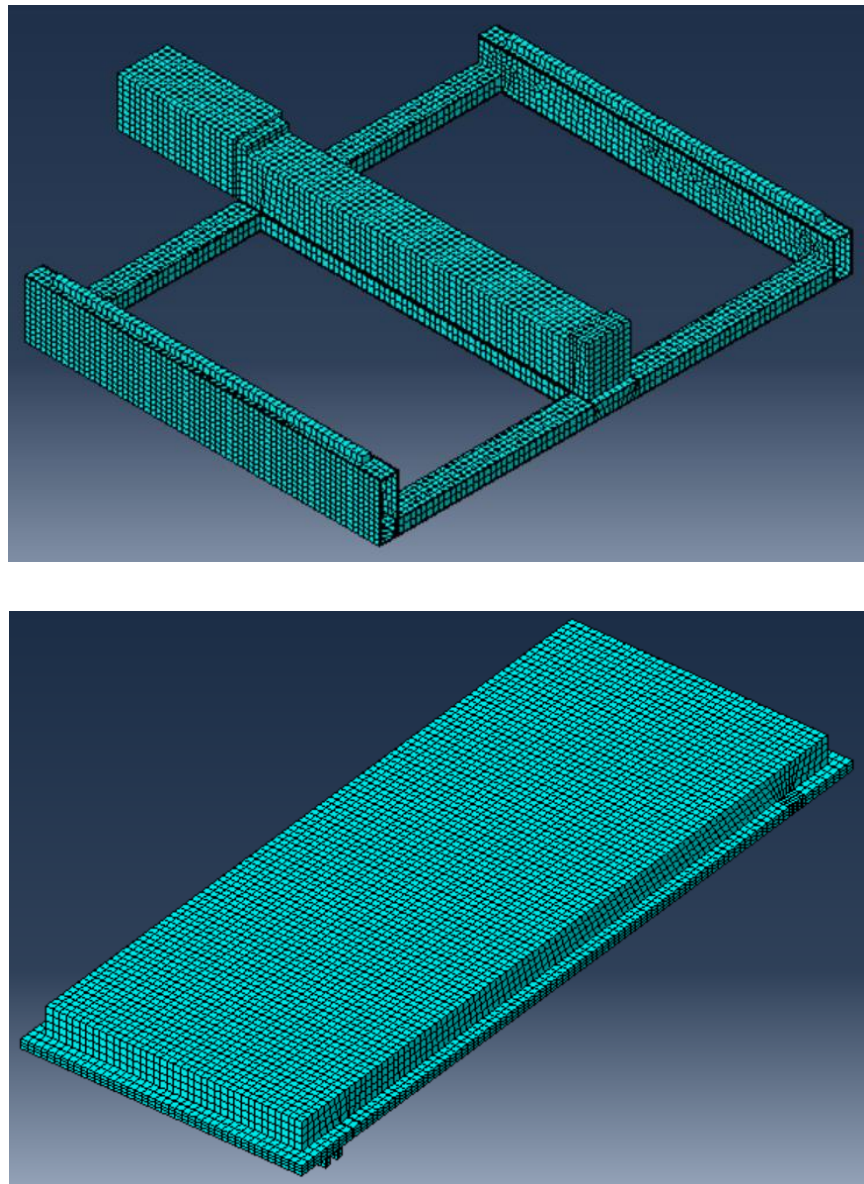


**Figure 33: Meshing of the supporting frame and vibrating plate**

### 3.5 Effect of standing subject

If a person is standing on the structure it may affect the vibrational behavior of the whole structure resulting in a particular resonance phenomenon where the perceived mass of the subject is different from the actual mass. This perceived value of the mass of the subject is the apparent mass and it should be considered to correctly evaluate the loading conditions. A model of the apparent mass of the human body is presented to determine if the dynamic behavior of the structure is affected by the subject standing on it. If the values of first natural frequencies of the two entities are distant on the spectrum they cannot affect each other and they are decoupled, but if their natural frequencies are close to each other, they can mutually excite and cause an overload on the structure.

To model the apparent mass of a standing subject the model 2a proposed by Matsumoto and Griffin [35] was used, where they propose to model the human body as two masses linked by a spring and dashpot, this scheme is showed in figure 34. The values of these parameters are based on the mean-normalized apparent masses of twelve subjects in standing posture. Since these values are mass normalized, it means that in order to get the actual values we need to multiply them by the static mass of the subjects. In our case we considered a mass of 100 Kg. The mass-normalized values of the parameters are showed in table 9.

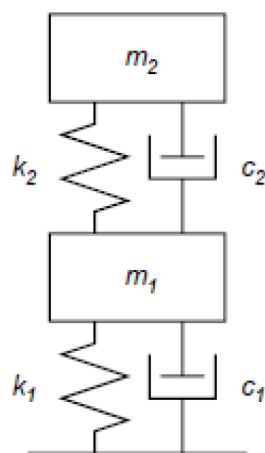


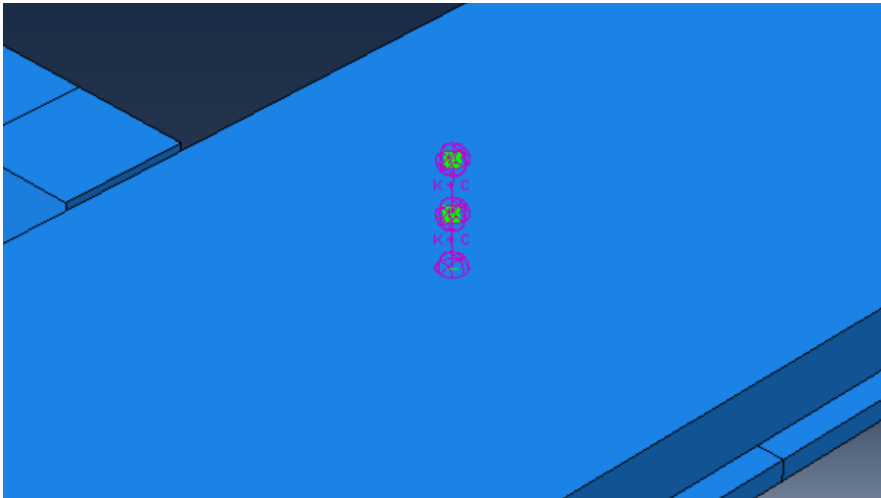
**Figure 34: Scheme of a standing human body**



Springs [N/m.Kg]		Dashpots [N.s/m.Kg]		Masses [-]	
k1	k2	c1	c2	m1	m2
4390	553	37.1	11.8	0.574	0.394

**Table 9: mass-normalized values of the parameters of the model**

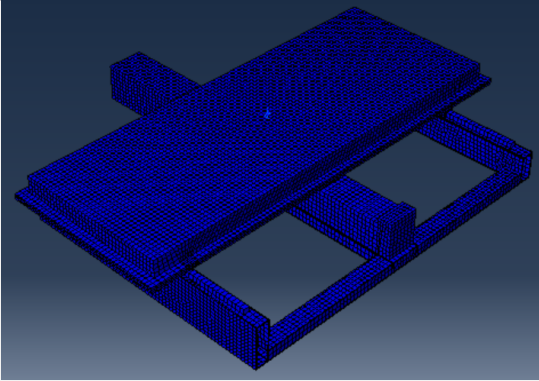
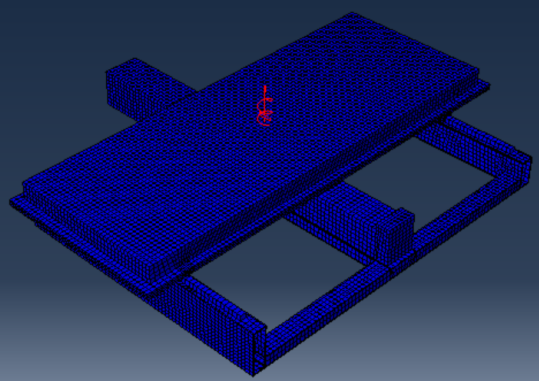
This model has been added to the model of the vibrating treadmill on Abaqus®, by adding a point instance in the center of the upper surface of the treadmill. Then it was constrained through a tie connection with the upper surface of the treadmill, two other points have been created in a vertical direction from the platform center. To add the parameter values, we need to multiply them by 100 Kg and take into account the units we are using in the FEM model previously showed in table 7. Then we add the values using the “special” tab on Abaqus® selecting the “Inertia” > “Point/mass inertia” command for the masses and selecting the “Springs/Dashpots” > “connect two points” command for the springs and dashpots. The model on the FEM structure is showed in figure 35.

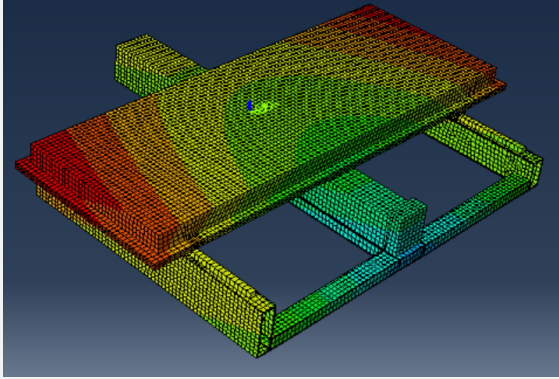
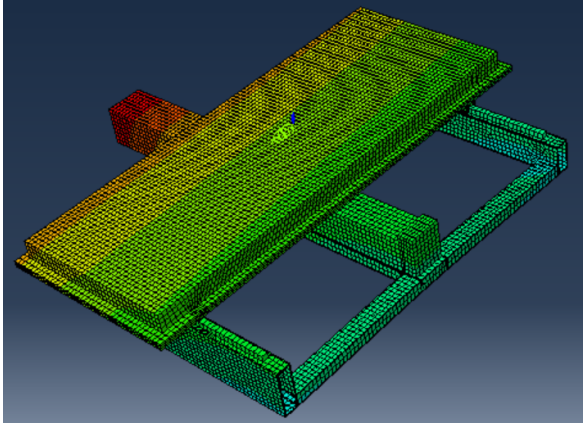
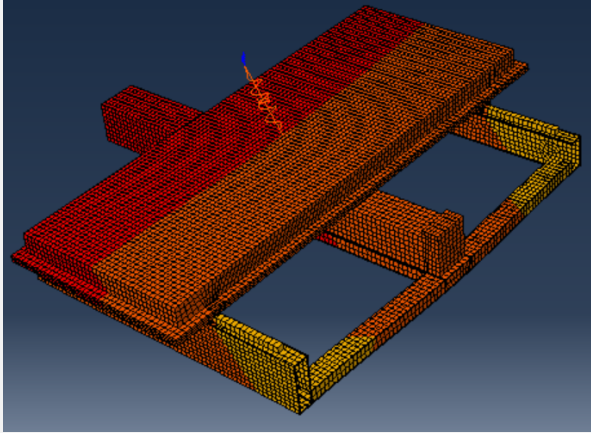


**Figure 35: FEM model of a standing subject**

### 3.6 FEM results

The first five modes obtained is showed in table 10 where we can see that the first two modes of vibration of the whole model correspond to the two modes of the standing subject at frequencies of 5.54 Hz and 14.67 Hz, as demonstrated by Griffin, while the first three modes of the machine occur at the frequencies of 46.12 Hz, 48.7 Hz and 56.72 Hz. This means that the modes of the structure and the standing subject are well decoupled and there is no mutual excitation. Furthermore, since the first modes of the structure occur at frequencies much higher than the maximum frequency imposed by the machine (10 Hz) we have a larger bandwidth meaning the structure would not reach resonance.

Mode number	Frequency	Mode shape
Mode 1	5.54 Hz	
Mode 2	14.67 HZ	

<p>Mode 3</p>	<p>46.12 Hz</p>	
<p>Mode 4</p>	<p>48.7 Hz</p>	
<p>Mode 5</p>	<p>56.72 Hz</p>	

**Table 10: Vibration modes of vibrating treadmill and standing subject**

# Chapter 4

## Preliminary performance analysis of the machine

An analysis has been done to the manufactured machine to test its performance. The machine is tested without the treadmill mounted on the vibrating platform. In this chapter the measurement set-up is presented as well as the results obtained.

### 4.1.1 Harmonic analysis of the actuated platform

To ensure that the plate was rigid enough for the vibration tests, four linear accelerometers with a sensitivity of 100 mV/g were positioned at the four corners of the vibrating plate, measuring in the direction of movement which can be seen in figure 36. Measuring the acceleration of the plate on its four corners allows us to ensure that there is no difference in output signal at each extremity. Any difference found in the output signal at any of the corners would imply that the plate was not rigid enough for the lateral vibration tests.

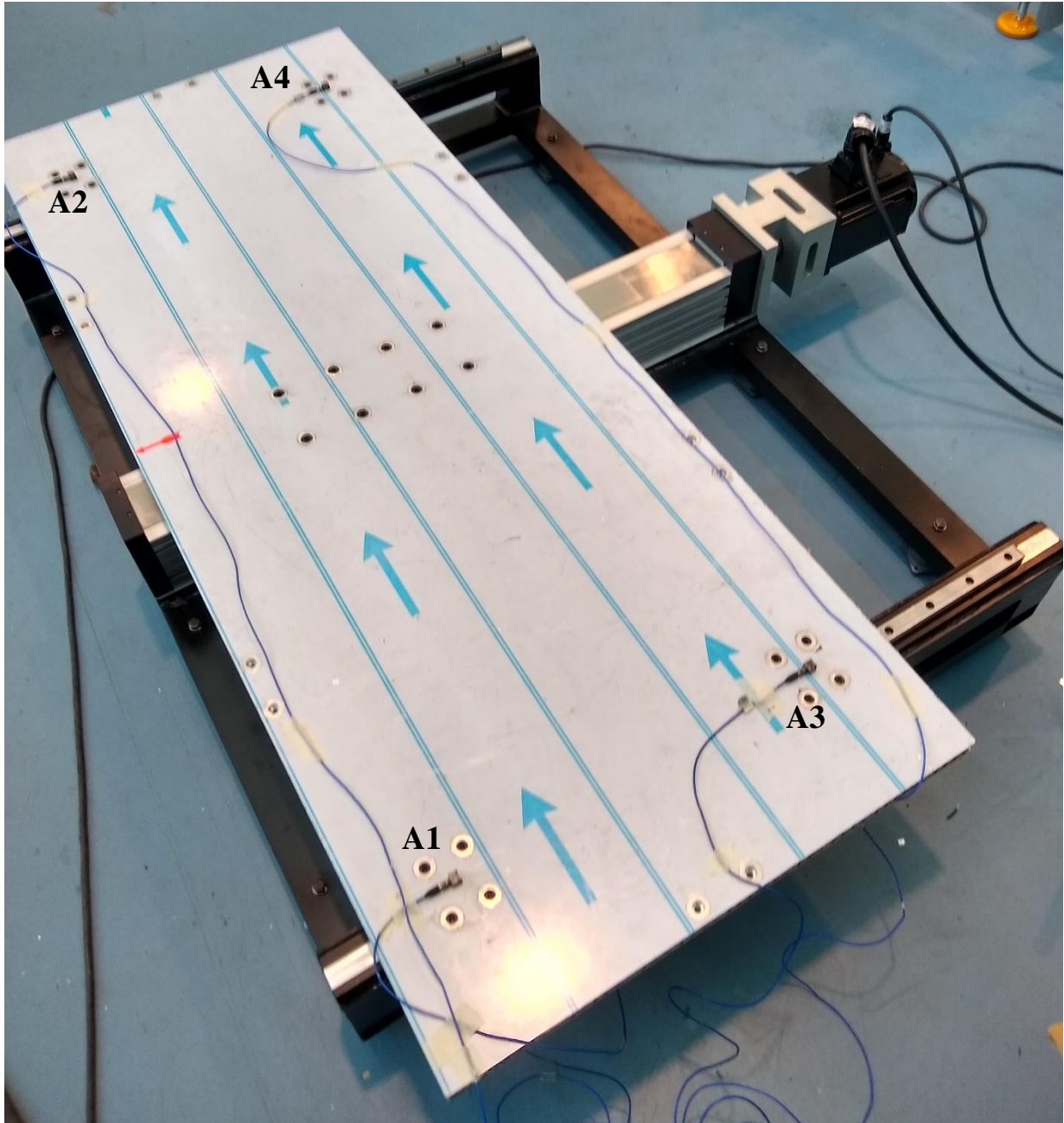


**Figure 36: Location of the accelerometers on the plate**

The four accelerometers have been connected to the four channels of a National Instruments 9234 acquisition board (figure 37). Data were sampled at 2048 Hz and acquired by a custom built software developed in LabVIEW.



**Figure 37: Nationals Instruments' 9234**

The input signals were a sine waves with different frequencies between 0.5-10 Hz and amplitudes of 2-60 mm, generated by a Keysight 33210A signal generator (figure 38).



**Figure 38: Keysight 33210A signal generator**

### 4.1.2 Set-up for three axis frequency response

To measure the acceleration response in all three axis to the acceleration input of the machine, one accelerometer (A4X) was located in the middle of the plate, that is where the slider of the actuator is connected and the three others (A1X, A2Z, A3Y) were connected in one corner in all three directions. A representation of this set-up is presented in figure 43.

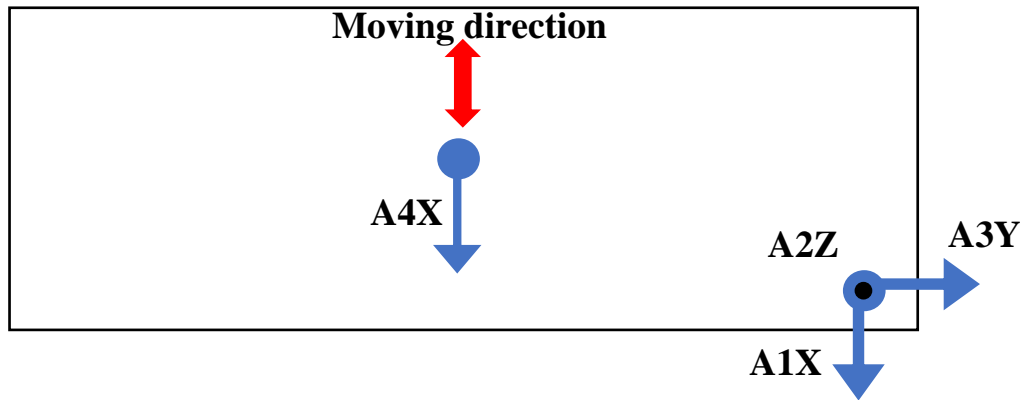


**Figure 43: Representation of the location of the accelerometers**

The acquisition of the data has been done with the same devices as the previous analysis.

### 4.2.1 Methodology for the harmonic analysis

In the first platform analysis a sine wave input signal was given to the motor with frequencies between 0.5 and 10 Hz and amplitudes between  $\pm 2$  and  $\pm 60$  mm. The different tests performed are showed in table 11.

Test name	Frequency [Hz]	Amplitude [mm]
F0_5A0_5	0.5	20
F1_0A0_5	1	20
F1_5A0_5	1.5	20
F2_0A0_5	2	20
F2_5A0_5	2.5	20
F3_0A0_5	3	20
F3_5A0_5	3.5	20
F4_0A0_5	4	20

<b>F0_5A1_0</b>	0.5	40
<b>F1_0A1_0</b>	1	40
<b>F1_5A1_0</b>	1.5	40
<b>F2_0A1_0</b>	2	40
<b>F2_5A1_0</b>	2.5	40
<b>F3_0A1_0</b>	3	40
<b>F3_5A1_0</b>	3.5	40
<b>F4_0A1_0</b>	4	40
<b>F0_5A1_5</b>	0.5	60
<b>F1_0A1_5</b>	1	60
<b>F1_5A1_5</b>	1.5	60
<b>F2_0A1_5</b>	2	60
<b>F5_0A0_1</b>	5	4
<b>F6_0A0_1</b>	6	4
<b>F5_0A0_05</b>	5	2
<b>F7_0A0_05</b>	7	2
<b>F10_A0_05</b>	10	2

**Table 11: Tests performed for harmonic analysis**

#### 4.2.2 Methodology for the three-axis frequency response

For this analysis, the input signals were sine waves with frequencies of 1, 2, 3 and 4 Hz and an amplitude of  $\pm 20$  mm and waves with frequencies of 5, 7 and 10 Hz with amplitudes of  $\pm 4$  mm. All the tests are named in table 12. The acquisition system was the same described in the previous analysis. Time signals were acquired, and the frequency response functions (FRF) between the triaxial measuring point and A4X accelerometer were computed with the software developed in LabVIEW.

<b>Test name</b>	<b>Frequency [Hz]</b>	<b>Amplitude [mm]</b>
<b>FRF_1_0A0_5</b>	1	$\pm 20$
<b>FRF_2_0A0_5</b>	2	$\pm 20$
<b>FRF_3_0A0_5</b>	3	$\pm 20$
<b>FRF_4_0A0_5</b>	4	$\pm 20$
<b>FRF_5_0A0_1</b>	5	$\pm 4$
<b>FRF_7_0A0_1</b>	7	$\pm 4$
<b>FRF_10_0A0_1</b>	10	$\pm 4$

**Table 12: Tests performed for the frequency response analysis**



### 4.3.1 Results and discussion of harmonic analysis

The acquired signals were processed using software developed in LabVIEW to extract the time domain and power spectra of the signals. In figures 39, 40 and 41 the output acceleration signals obtained for frequencies of 1, 2, 3 Hz with an amplitude of  $\pm 20$  mm and filtered with a Butterworth 4<sup>th</sup> order filter at 30 Hz are shown.

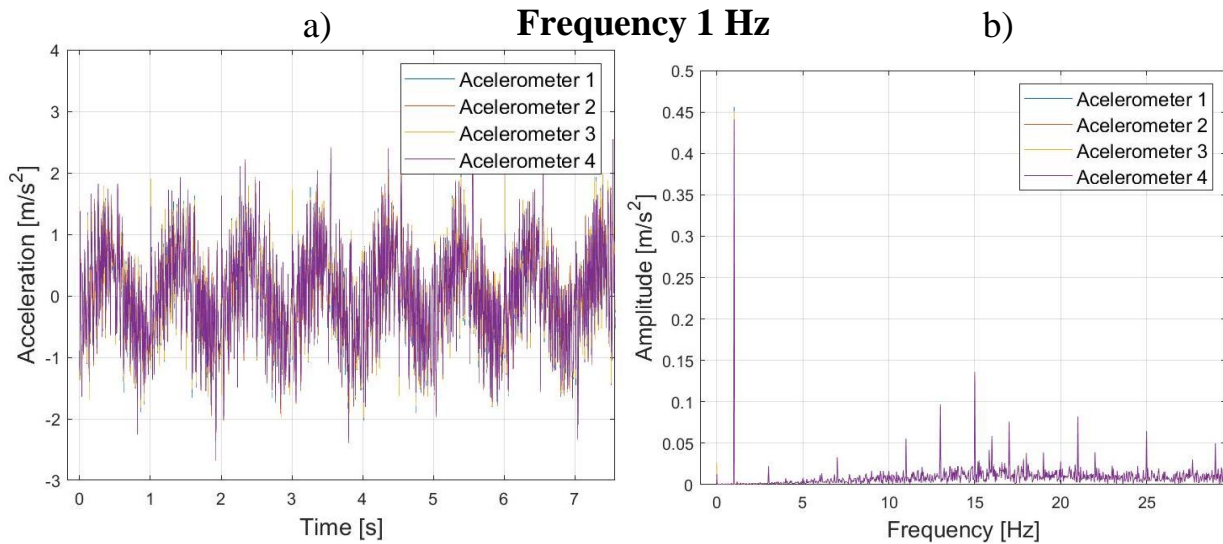


**Figure 39: a) Time domain and b) Power spectra with 1Hz  $\pm 20$  mm input**

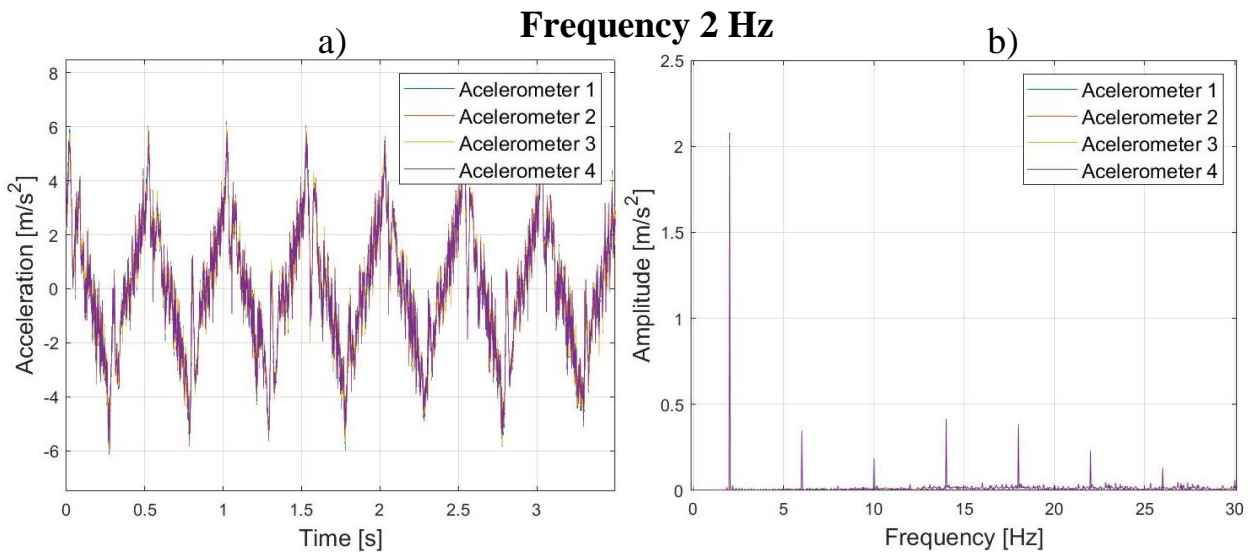


**Figure 40: a) Time domain and b) Power spectra with 2Hz  $\pm 20$  mm input**

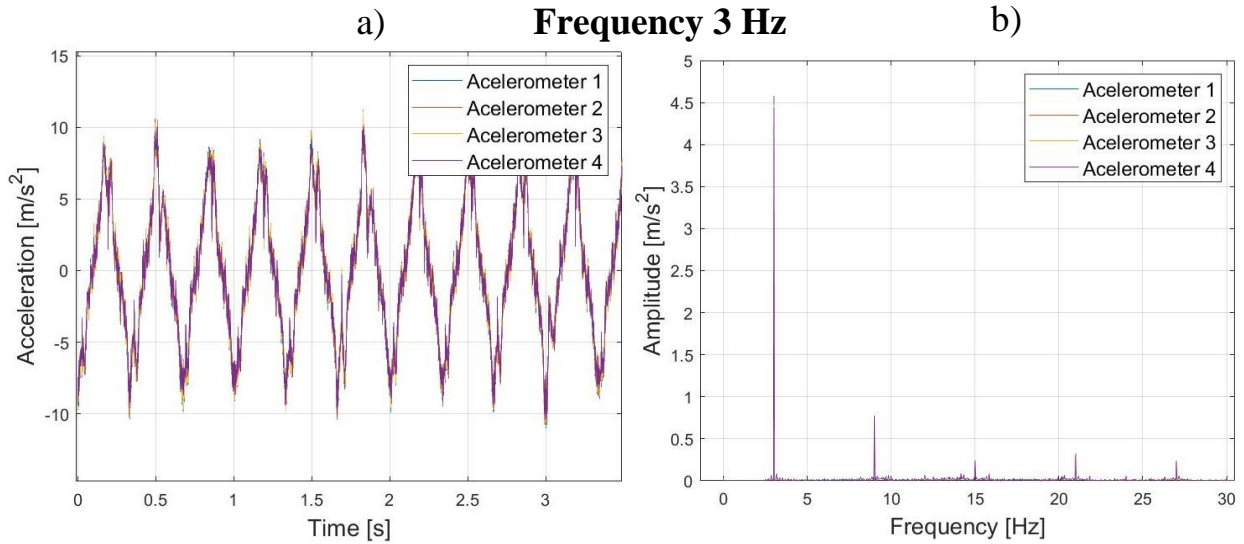


**Figure 41: a) Time domain and b) Power spectra with 3Hz ± 20 mm input**

As shown in the time domain of the signals, the four accelerometers located in each corner are in phase and have almost the same acceleration meaning the plate is rigid enough. There is also the presence of noise seen in the time domain graphs and the presence of higher harmonics on the power spectra, this can be due to noise coming from the industrial environment. Total harmonic distortion (THD) has been calculated using MATLAB for all the signals. The THD gives a value in dB of how much lower the first six harmonics are in comparison to the fundamental frequency. The THD between the four accelerometers is computed for each test and is showed in figure 42.

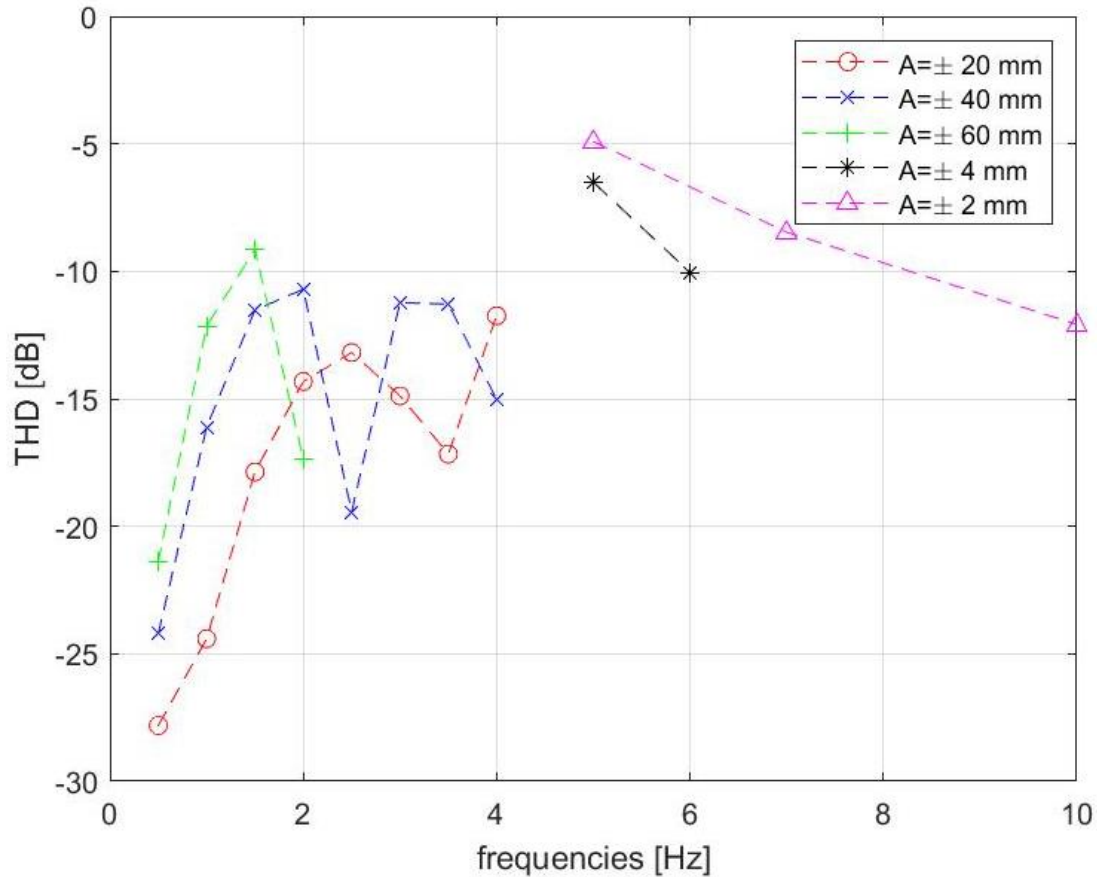


**Figure 42: Total harmonic distortion for all signals**

At 0.2 Hz with 20 mm amplitude the THD is -27 dB, meaning the multiple harmonics magnitude is limited compared with the fundamental frequency. With increasing frequency, the harmonics magnitude increases.

### 4.3.2 Results and discussion of the Frequency response analysis

To obtain the FRF the signal obtained by the accelerometer A4X was considered the stimulus while the other three the responses. In figure 44 the modulus, phase and coherence of the 4 Hz with  $\pm 20$  mm amplitude input signals is presented.

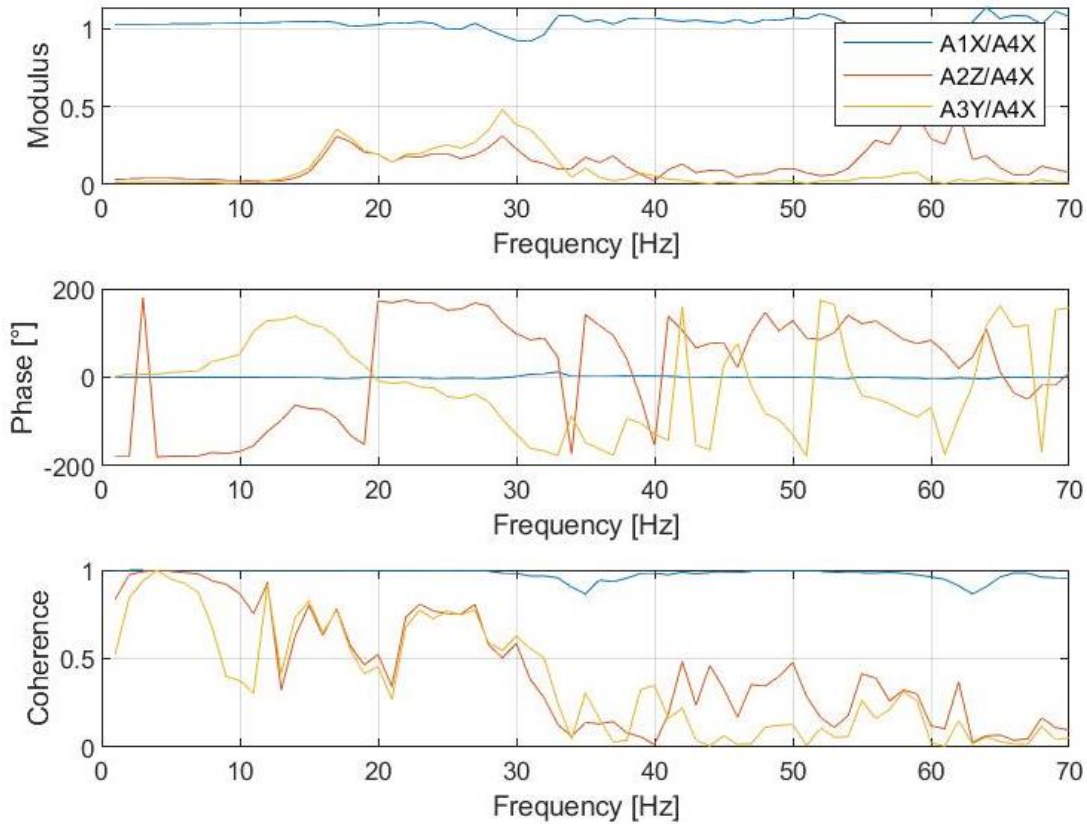


**Figure 44: FRF of the sine wave with 4 Hz frequency and  $\pm 20$  mm amplitude**

It can be seen that the modulus of the FRF of the signal of the accelerometers with the same direction A1X/A4X is unitary below 30 Hz, which means that with an acceleration input in the middle of the plate we get the same acceleration output in the corner of the plate. The modulus of the FRF of the accelerometers with the other directions, A2Z/A4X and A3Y/A4X is approximately zero in frequencies lower than 12 Hz, which means that an acceleration input in the X direction with a frequency lower than 12 Hz would not produce any acceleration in the other directions.

# Chapter 5

## Cognitive test

The cognitive tests and the protocol that will be used to perform the experiments on the subjects will be presented as well as the design of the device used to run the PVT test. Finally, the results from the testing of a prototype of the PVT device are discussed.

### 5.1 Method and protocol

The protocol design tests the cognitive performance of subjects before, during and after exposure to medio lateral vibration, as well as, having a control group of people that will not be exposed to vibration. This group of people will perform the cognitive tests before walking, then will perform a PVT test while walking without any vibration and a final test after walking. These two groups have been decided to determine the influence of the exposure to vibrations on the cognitive performance, while controlling for the possible effects of fatigue due to walking.

The cognitive tests performed will be a Stroop test and a PVT test, the second one being possible to be done while walking. The sequence of testing for the different groups is presented in figure 45.



**Figure 45: Sequence for testing for the different groups**

The PVT tests will last five minutes where each minute has random interval times between the stimuli and the sequence of minutes is randomized in each trial. Each time the subject takes the PVT test with vibrations, the frequency of them is changed, to test the influence in cognitive performance of different frequencies.

The three Stroop tests will last one minute and will consist of ten stimuli each. the baseline Stroop will be a visual reaction test where the subject needs to press a button as soon as a visual stimulus in a monitor occurs. The second Stroop is performed after the first walk, and the subject must indicate if the color of the word matches or not the word meaning. The third Stroop test is done after a second walk, and the subject must indicate if the color of the word mismatches or not the word meaning.

## 5.2 PVT testing design

Since the subject will be performing the PVT while walking an audible stimulus will be used for the testing. The subject will have headphones to hear the stimulus and an ergonomic joystick with one button, that needs to be pressed when the stimulus happens.

The button selected is the CANFORD® push button (figure 46) that has an ergonomic shape to hold with one hand.



**Figure 46: CANFORD® push button**

The testing consists of trials of five minutes, with ten audible stimuli each minute separated by random time intervals, the sequence of minutes is also randomized in each trial. The controller used to run the test will be an Arduino® WEMOS D1 mini (figure 47), that will run the tests, measure the reaction time and send via Wi-Fi the results of each trial to a computer, where the data will be processed.



**Figure 47: Arduino® WEMOS D1 mini controller**

The WEMOS will be fixed on a PCB board housed on a 3D printed plastic case. This case is presented in figure 48, where the four holes a4) are used to fix the PCB board with the WEMOS and the required connections, the four holes b4) are used to fix the lid

of the housing, the aperture c4) is used to connect the power supply to the WEMOS and the hole d4) is used for the cables that exit the housing such as the ones that connect the button and the headphones.

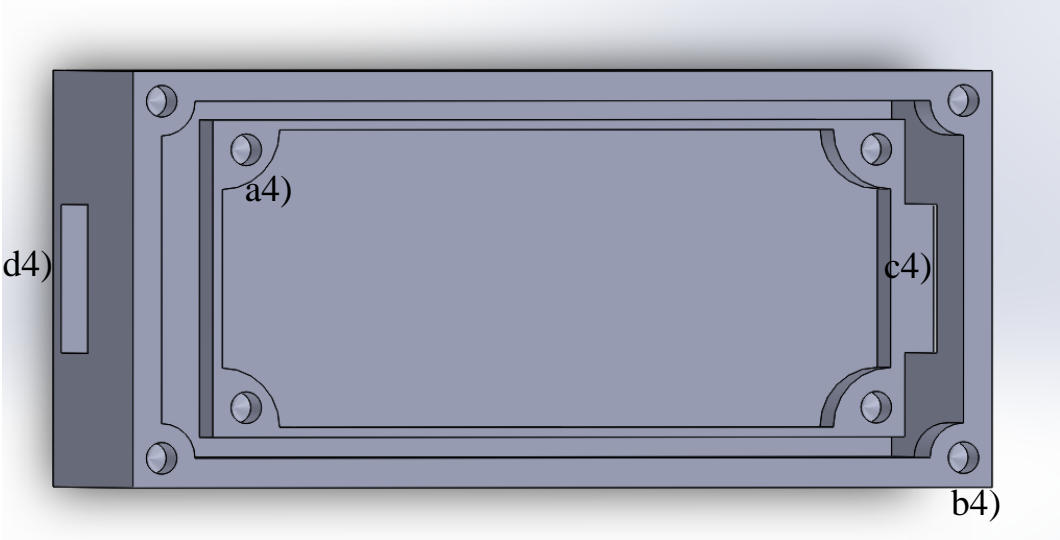


**Figure 48: Case of the WEMOS' housing**

The lid for the housing is presented in figure 49, where the four holes a5) are used to fix it to the case and in the two holes b5) there will be two LEDs that will give information to the tester if the PVT test is working correctly.

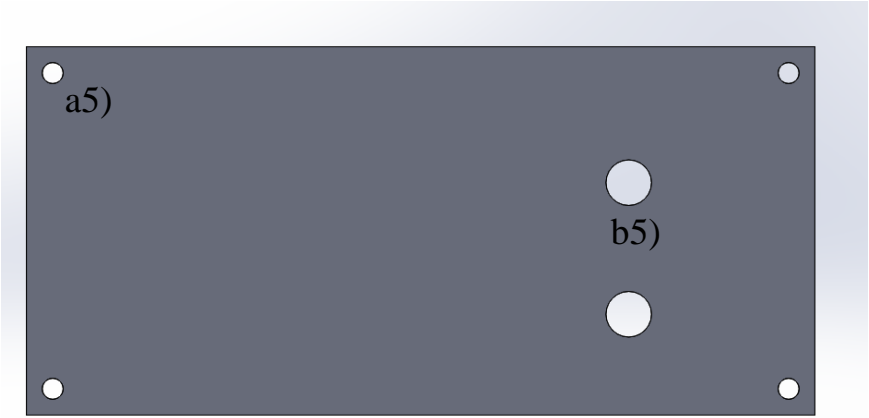


**Figure 49: Lid of the WEMOS' housing**

**5.3 PVT testing prototype**

To test the functionality of the device a prototype on a protoboard was made, showed in figure 50, where the WEMOS (a6) is connected to a button (b6) and a buzzer



(c6) that gives the audible stimulus instead of the headphones. The two LEDs (d6) give an indication if the test is running correctly.

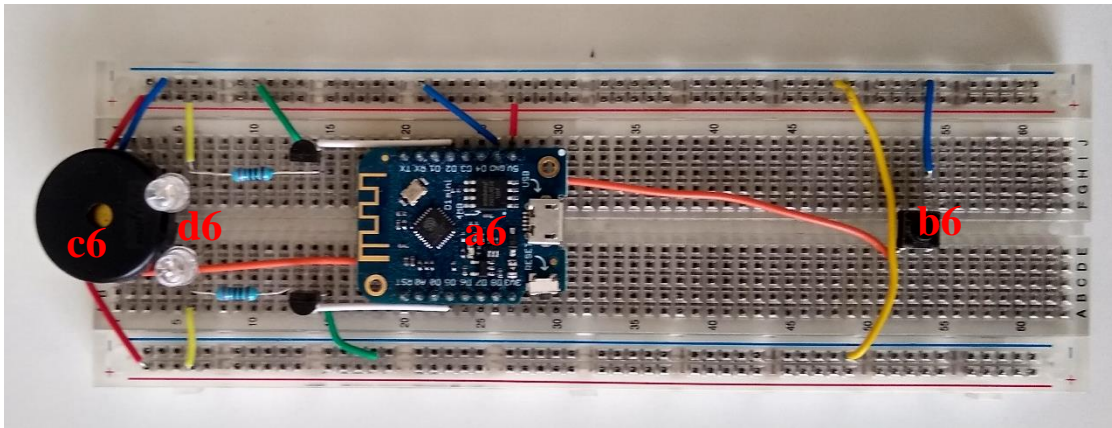


**Figure 50: PVT testing prototype**

### **5.3.1 Method**

Four seated subjects were tested using the prototype previously shown. They performed three trials of five minutes each of PVT testing. Each trial was divided in 5 minutes with the randomized time intervals for the audible stimulus, the sequence of these minutes was randomized as well for each trial, so the subjects would all take the same test but in a random order. The aim of this preliminary test was to determine if there is a training or fatigue factor when performing a prolonged test. All subjects made one trial with their eyes closed, to test if visual stimulus influences their response times.

### **5.3.2 Results and discussion**

The reaction time to the stimuli of each subject was saved on a computer and processed using MATLAB to plot the average reaction time of each minute of all the trials for the four subjects, an example for subject one is presented in figure 51. Since the button was not so ergonomic, sometimes when pressed, it would not be counted, when this happened the values were discarded.

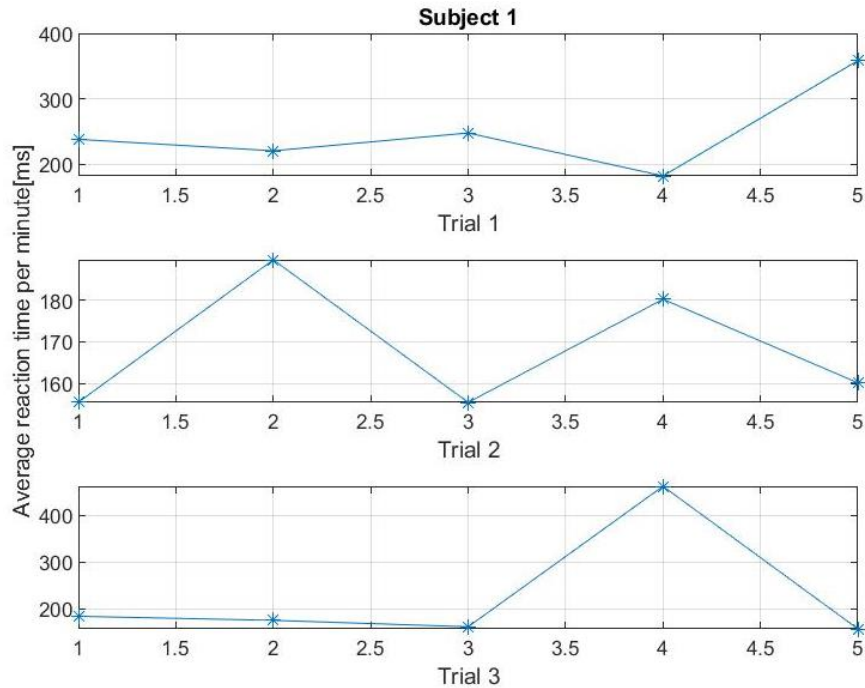


**Figure 51: Subject's 1 average reaction time in each minute**

Since there is not a clear increase or decrease of the reaction time throughout the trials, there is no appreciable training or fatigue factor on the subjects. Then, the reaction time of each trial was averaged for all subjects, in figure 52 the graph for subject one is showed.

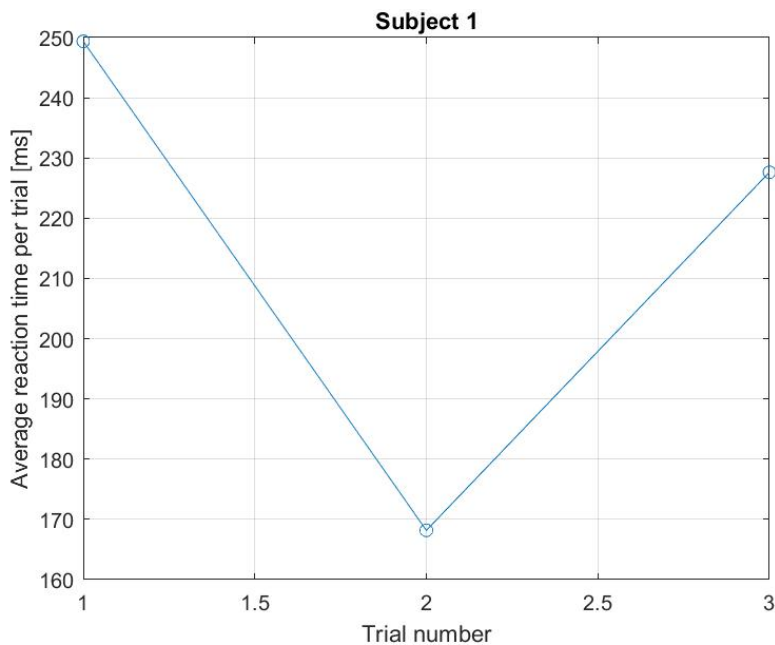


**Figure 52: Subject's 1 average reaction time in each trial**

The subject one had his eyes closed on trial number 2, which coincides with the trial with lower reaction time, this happened on three of the four subjects tested, meaning that there could be an influence if the subject has or not their eyes opened. Therefore, it is suggested that the subjects have their eyes opened during testing to ensure that testing parameters while walking are similar to those during rest.

Finally, the average reaction time of all the subjects in each trial and the deviation is shown in figure 53.

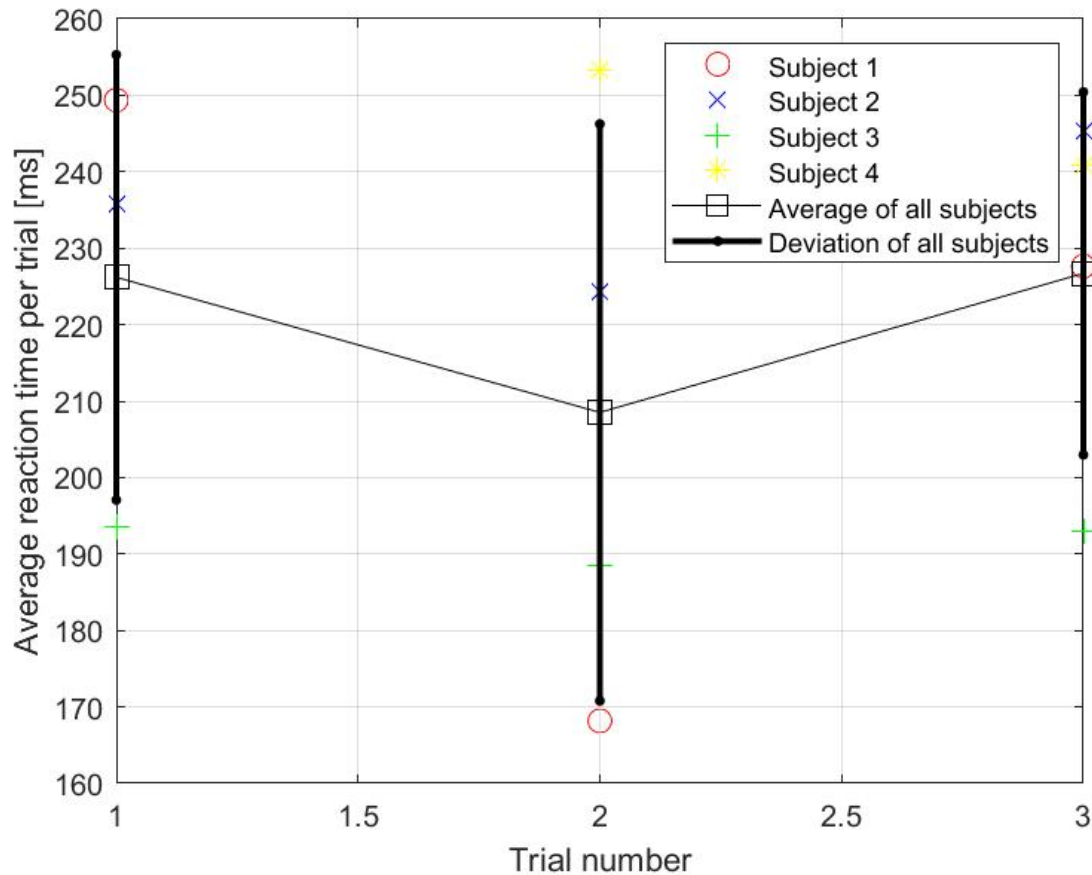


**Figure 53: Average and deviation of the reaction time in each trial**

This graph is useful to visualize the relation between the mean and the standard deviation of the reaction time between trials. Since, the standard deviation is large compared to the difference of the mean, there is not a statistical significant result to determine that there is a training factor between trials, so the results of every trial could be compared with each other. Then, during the actual cognitive testing, if the subject has its eyes opened and is fully concentrated on the test, and there is a significant difference

between the trials, then the difference could be due to the vibration exposure of the subject or to walking fatigue.

# Chapter 6

## Conclusions and future developments

### 6.1 Conclusions

In this thesis a lightweight, portable, single axial shaker has been designed and constructed with the primary objective of being able to support a person walking on a treadmill. The shaker has been analyzed using FEA to understand possible modes of vibration of the structure. The first were found at approximately 5 and 14 Hz which correspond to the modes of a standing person, while the first modes related to the structure are around 46 and 48 Hz.

From the preliminary performance analysis of the machine, it can be concluded that the plate is rigid enough for the bandwidth requested, since the signal from all four accelerometers were on phase. The output signal on the accelerometers measured the main sinusoidal input plus higher harmonics with low energy contribution in respect to the main frequency.

The PVT test was tested, and the protocol was validated to test the influence of vibration standing on the floor and on the vibrating platform.

### 6.2 Future developments

In order to validate and compare the results obtained from the FEM modal analysis, an experimental modal analysis should be done by doing an impulse test with an impact hammer and measuring the acceleration on certain points of the structure depending on the modal shapes of the structure.

An ergonomic button for the PVT test should be used in order to reduce the number of outliers and it was shown that the subjects when being tested should have their eyes opened and give their full attention to the test so the results could be compared fairly.

# Bibliography

- [1] P. Nataletti, E. Marchetti, A. Lunghi and others, "Occupational exposure to mechanical vibration: the Italian vibration database for risk assessment," *International Journal of Occupational Safety and Ergonomics*, vol. 14, no. 4, pp. 379-386, 2008.
- [2] C. Bosco *et al*, "Hormonal responses to whole-body vibration in men," *Eur. J. Appl. Physiol.*, vol. 81, (6), pp. 449-454, 2000.
- [3] N. Wei *et al*, "Optimal frequency/time combination of whole-body vibration training for improving muscle size and strength of people with age-related muscle loss (sarcopenia): A randomized controlled trial," *Geriatrics & Gerontology International*, vol. 17, (10), pp. 1412-1420, 2017.
- [4] M. Shafiquzzaman Khan and Jerker Sundstrom "Effects of vibration on sedentary activities in passenger trains" *Journal of low frequency noise, vibration and active control*, pp. 43-55
- [5] International Standards Organisation, "Evaluation of Human Exposure to Whole-body Vibration. Part 1-General Requirements. ISO2631. 1," 1997.
- [6] M. Bovenzi, M. Schust and M. Mauro, "An overview of low back pain and occupational exposures to whole-body vibration and mechanical shocks," *Med. Lav.*, vol. 108, (6), pp. 419-433, 2017.
- [7] L. Burström, T. Nilsson and J. Wahlström, "Whole-body vibration and the risk of low back pain and sciatica: a systematic review and meta-analysis," *Int. Arch. Occup. Environ. Health*, vol. 88, (4), pp. 403-418, 2015.
- [8] European Agency for Safety and Health at Work, *OSH in figures - Work-related musculoskeletal disorders in the EU - Facts and figures*, Luxembourg, 2010.
- [9] Massimo Bovenzi, "A longitudinal study of low back pain and daily vibration exposure in professional drivers" *Industrial Health*, vol. 48, pp. 584–595, 2010.
- [10] Gülin Birlik, "Occupational Exposure to Whole Body Vibration-Train Drivers" *Industrial Health*, vol. 47, pp. 5–10, 2009.
- [11] Ghi Chan Kim. "Degenerative Changes of Spine in Helicopter Pilots" *Department of Physical Medicine & Rehabilitation, Kosin University*, 2013.
- [12] N. Shibata, "Subjective response of standing persons exposed to fore-aft, lateral and vertical whole-body vibration," *International Journal of Industrial Ergonomics*, vol. 49, pp. 116-123, 2015.

- [13] G. H. M. J. Subashi, Y. Matsumoto and M. J. Griffin, "Apparent mass and cross-axis apparent mass of standing subjects during exposure to vertical whole-body vibration," *Journal of Sound and Vibration*, vol. 293, pp. 78-95, 2006.
- [14] H. V. Dang and S. Živanović, "Influence of Low-Frequency Vertical Vibration on Walking Locomotion" *Journal of structural engineering*, vol. 142 (12), 2016.
- [15] J. A. Nessler, S. Heredia, J. Bélair, J. Milton, "Walking on a Vertically Oscillating Treadmill: Phase Synchronization and Gait Kinematics" *PLoS ONE 12(1)*, 2017.
- [16] M. Basner, D. Mollicone, and D. F. Dinges, "Validity and Sensitivity of a Brief Psychomotor Vigilance Test (PVT-B) to Total and Partial Sleep Deprivation" *Acta Astronautica*, vol.69 (11-12), pp 949-959, 2011
- [17] I. Lee, W. A. Bardwell, S. A. Israel, and J. E. Dimsdale, "Number of Lapses during the Psychomotor Vigilance Task as an Objective Measure of Fatigue" *Journal of clinical sleep medicine*, vol.6 (2), pp 163-168, 2010.
- [18] M.J.M. Lamers, A. Roelofs, and I.M. Rabeling-Keus, "Selective attention and response set in the Stroop task." *Memory & Cognition* 38, pp. 893–904, 2010.
- [19] J. Roesch, "Electrodynamic vs Hydraulic Shakers: Which is best for your product?," Austin Reliability Labs, 2019. [Online]. Available: <https://www.austinrl.com/electrodynamic-vs-hydraulic-shakers-which-is-best-for-your-product/>.
- [20] A. Fontanieri, *Bandwidth-optimized force platform for a multiaxial shaker*, Politecnico di Milano: M. Sc. thesis, 2019.
- [21] T. Cloete and C. Scheffer, "Benchmarking of a full-body inertial motion capture system for clinical gait analysis," 2008, *30th Annual International Conference of the IEEE Engineering in Medicine and Biology Society*, Vancouver, pp. 4579-4582, 2008.
- [22] A. Pfister, A. M. West, S. Bronner and J. A. Noah, "Comparative abilities of Microsoft Kinect and Vicon 3D motion capture for gait analysis", *Journal of Medical Engineering & Technology*, vol. 38 (5), pp. 274-280, 2014.
- [23] Z. S. Nasreddine, N. A. Phillips, V. Bedirian, S. Charbonneau, V. Whitehead, I. Collin, J. L. Cummings, and H. Chertkow, "The Montreal Cognitive Assessment, MoCA: A Brief Screening Tool For Mild Cognitive Impairment", *J Am Geriatr Soc*. Vol 53(4), pp. 695-699. 2005.
- [24] J. Ljungberg, G. Neely, R. Lundström, "Cognitive performance and subjective experience during combined exposures to whole-body vibration and noise", *Int Arch Occup Environ Health*. Vol 77(3), pp. 217-221, 2004.
- [25] N. Costa, P. M. Arezesa, R. B. Melo, "Effects of vibration exposure on professional drivers: a field test for quantifying visual and cognitive performance", 41 Suppl 1 pp. 3039-3042, Work. 2012.

- [26] D. Stamenković, V. M. Popovic, M. Tirovic, “Operator's reaction time prolongation induced by whole-body vibration”, *FME Transactions*, vol. 42(4), pp.297-304, 2004.
- [27] Z. Zamanian, A. Nikraves, M. R. Monazzam, J. Hassanzadeh and M. Fararouei, “Short-term exposure with vibration and its effect on attention”, *Journal of Environmental Health Science & Engineering* 2014, 12:135.
- [28] A. Azizan, Z. Zali, and H. Padil, “Evaluation of reaction time performance and subjective drowsiness during whole-body vibration exposure”, *IOP Conf. Ser.: Mater. Sci. Eng.* 370, 2018.
- [29] A. B. Fuermaier, L. Tucha, J. Koerts et al. “Good vibrations--effects of whole body vibration on attention in healthy individuals and individuals with ADHD.” *PLoS One*, vol 9(2), 2014.
- [30] M. Yung, A. E. Lang, J. Stobart, A. M. Kocielek, S. Milosavljevic, C. Trask “The combined fatigue effects of sequential exposure to seated whole body vibration and physical, mental, or concurrent work demands.” *PLoS One*. Vol 12(12), 2017.
- [31] L. Burström, T. Nilsson and J. Wahlström, “Whole-body vibration and the risk of low back pain and sciatica: a systematic review and meta-analysis.” *Int Arch Occup Environ Health* vol. 88, pp. 403–418, 2015.
- [32] H. Giberti, S. Cinquemani and G. Legnani, “Effects of transmission mechanical characteristics on the choice of a motor-reducer” *Mechatronics* vol.20-5, pp. 604-610, 2010.
- [33] M. Tarabini, S. Solbiati, B. Saggin, D. Scaccabarozzi, “Apparent mass of standing subjects exposed to multi-axial whole-body vibrations” *Ergonomics* vol. 59-8, pp. 1038-1049, 2016.
- [34] P. Marzaroli, *Development of tools and systems for the protection of workers from foot-transmitted whole-body vibration*, Politecnico di Milano: Phd thesis, 2019.
- [35] Y. Matsumoto and M. J. Griffin, *Mathematical models for the apparent masses of standing subjects exposed to vertical whole-body vibration*, *Journal of Sound and Vibration*, vol. 260, pp. 431-451, 2003.



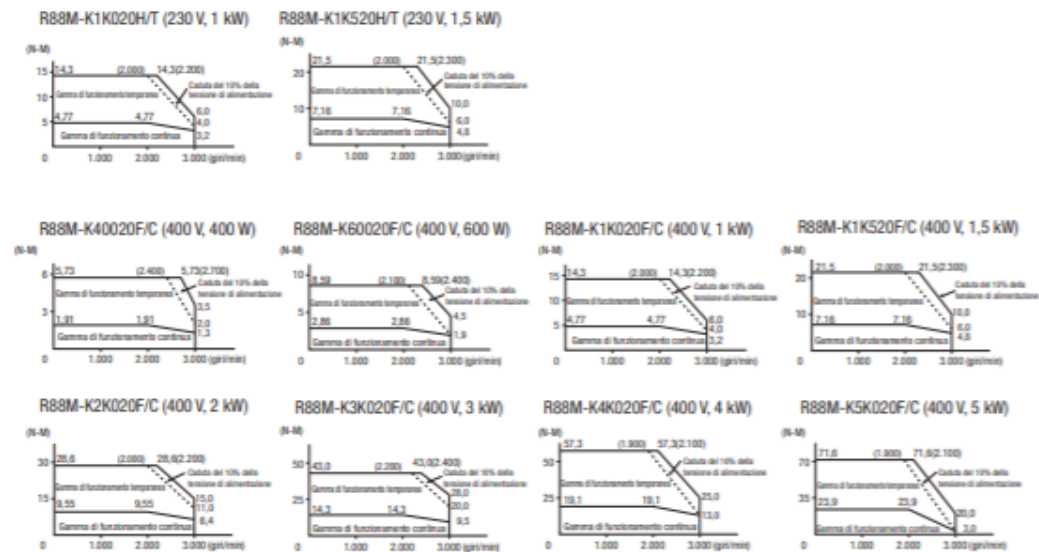
# Appendix

## [A.1] Data sheet

Tensione		230 V				400 V					
Modello servomotore R88M-K...	Incrementale a 20 bit Assoluto a 17 bit	1K020H- 1K020T-	1K520H- 1K520T-	0020F- 0020C-	60020F- 60020C-	1K020F- 1K020C-	1K520F- 1K520C-	2K020F- 2K020C-	3K020F- 3K020C-	4K020F- 4K020C-	5K020F- 5K020C-
Potenza nominale	W	1.000	1.500	400	600	1.000	1.500	2.000	3.000	4.000	5.000
Coppia nominale	N·m	4,77	7,16	1,91	2,86	4,77	7,16	9,55	14,3	19,1	23,9
Coppia massima istantanea	N·m	14,3	21,5	5,73	8,59	14,3	21,5	28,7	43	57,3	71,6
Corrente nominale	A (rms)	5,7	9,4	1,2	1,5	2,8	4,7	5,9	8,7	10,6	13
Corrente massima istantanea	A (rms)	24	40	4,9	6,5	12	20	25	37	45	55
Velocità nominale	min <sup>-1</sup>	2.000									
Velocità massima	min <sup>-1</sup>	3.000									
Costante di coppia	N·m/A	0,63	0,58	1,27	1,38	1,27	1,16	1,27	1,18	1,40	1,46
Momento di inerzia del rotore (JM)	kg·m <sup>2</sup> ×10 <sup>-4</sup> (senza freno)	4,60	6,70	1,61	2,03	4,60	6,70	8,72	12,9	37,6	48
	kg·m <sup>2</sup> ×10 <sup>-4</sup> (con freno)	5,90	7,99	1,90	2,35	5,90	7,99	10	14,2	38,6	48,8
Momento di inerzia massimo del carico (JL)	Multiplo di (JM)	10 <sup>1</sup>									
Potenza nominale	KW/s (senza freno)	49,5	76,5	22,7	40,3	49,5	76,5	105	159	97,1	119
	KW/s (con freno)	38,6	64,2	19,2	34,8	38,6	64,2	91,2	144	94,5	117
Carico radiale consentito	N	490									
Carico di spinta consentito	N	196									
Peso approssimativo	kg (senza freno)	5,2	6,7	3,1	3,5	5,2	6,7	8	11	15,5	18,6
	kg (con freno)	6,7	8,2	4,1	4,5	6,7	8,2	9,5	12,6	18,7	21,8
Caratteristiche del freno	Tensione nominale	24 Vc.c. ±10%									
	Momento di inerzia del freno di stazionamento	(J) kg·m <sup>2</sup> ×10 <sup>-4</sup> 1,35									
	Assorbimento di potenza (20°C)	W	14	19	17	14	19	22	31		
	Assorbimento di corrente (20°C)	A	0,59 ±10%	0,79 ±10%	0,70 ±10%	0,59 ±10%	0,79 ±10%	0,90 ±10%	1,3 ±10%	1,3 ±10%	
	Coppia attrito statico	N·m (minimo)	4,9	13,7	2,5	4,9	13,7	16,2	24,5		
	Tempo di salita per la coppia di stazionamento	ms (max.)	80	100	50	80	100	110	80		
Caratteristiche di base	Tempo di rilascio	ms (max.)	70	50	15	70	50	25			
	Time Rating	Continuo									
	Classe di isolamento	Tipo F									
	Temperatura ambiente di stoccaggio/esercizio	0... +40°C/-20... 65°C									
	Umidità relativa di stoccaggio/esercizio	20... 85% (senza formazione di condensa)									
	Classe di vibrazioni	V-15									
Resistenza di isolamento	Minimo 20 MΩ a 500 Vc.c. tra i terminali di alimentazione e il terminale FG										
Custodia	Internamente chiuso, autoraffreddato, IP67 (esclusa l'apertura dell'albero)										
Resistenza alle vibrazioni	Accelerazione vibrazioni 49 m/s <sup>2</sup>										
Montaggio	A flangia										

\*1. Inerzia carico applicabile: il coefficiente di inerzia del carico operativo (inerzia del carico/inerzia del rotore) dipende dalla configurazione meccanica e dalla relativa rigidità. Per una macchina a elevata rigidità, il funzionamento è possibile anche con un'inerzia del carico elevata. Selezionare un motore appropriato e confermare la possibilità di funzionamento.

### Caratteristiche coppia-velocità







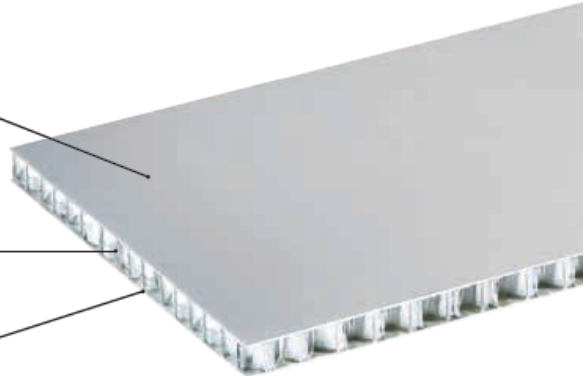
CEL Components S.r.l.  
Via Ca' dell'Orbo Sud 4 - 40055 Castenaso (Bologna) Italy  
Tel. +39 051 782605 Fax +39 051 782477  
www.cel.eu info@cel.eu  
P.IVA 04102800378 CCIAA BO 0339628  
ALUMINIUM AND THERMOPLASTIC HONEYCOMBS, LAMINATES, SANDWICH PANELS

ENG

## Compoce® AL

ALUMINIUM SKINS  
Thickness mm: 0,5 - 0,8 - 1 (standard)

CORE  
Aluminium honeycomb (Alloy series 3000\*) with hexagonal cells  
Diameter: Ø1/4", Ø3/8", Ø1/2", Ø3/4"  
Thickness Foil: from 50 to 70 microns



\* To Aluminium alloy series 3000 belong: Aluminium alloy 3003, Aluminium alloy 3005, Aluminium alloy 3103, Aluminium alloy 3104.

Technical data sheet for standard panels (dimensions, materials and special finishes on request)

		Technical data sheet for standard panels (dimensions, materials and special finishes on request)									
TECHNICAL CHARACTERISTICS OF PANEL	panel size	mm	standard 1250 x 2500 / 1250 x 3000 / 1500 x 3000; On request up to 2000 x 7000								
	thickness tolerance	mm	± 0,3								
	dimension's tolerance	mm	± 30								
	planarity ***	mm/m	+/- 1								
	skins' thickness	mm	from 0,5 to 5,0								
	skin aluminium alloy		1000 series, 3000 series, 5000 series								
	honeycomb aluminium alloy		3000 series, 5000 series								
	thickness of honeycomb foil	µm	50 and 70								
	diameter of honeycomb	Ø = mm	from 3 to 19								
	honeycomb density	Kg/m³	from 20 to 163								
adhesive		two-components polyurethane adhesive/thermoplastic film/ epoxy film/ two-components epoxy adhesive									
skin characteristics		rough/primer/polyester/PVDF/ anodised									
PANEL PHYSIC AND MECHANIC PERFORMANCES	type panel (some examples)	Panel Thickness mm	6	10	15	10	15	20	25		
		Skin Thickness mm	0,5 + 0,5			1,0 + 1,0					
	panel weight ‡	Kg/m²	3,8	4,0	4,3	6,7	7,0	7,3	7,6		
	compressive stabilised strength MPa ** ‡	ASTM C 365-365 M	Mpa	2,9							
	maximum load ** ‡	ASTM C 393 †	N	190	340	520	600	1.000	1.350	1.700	
	deflection at maximum load ‡	ASTM C 393 †	mm	14	8	6	8	6	4	3	
	skins E Elastic Modulus		Mpa	68.000 - 70.000							
	moment of inertia I **		mm⁴/m	7.600	22.000	52.000	40.000	98.000	181.000	288.000	
	average resistance to peeling ** ‡	ASTM D1781-98 (2012)		> 280 N/76 mm or 40 Nmm/mm							
	maximum service temperature **		°C	- 40 / + 60; on request + 80 / + 100 / + 150							
thermal expansion coefficient **		°C <sup>-1</sup>	2,3 x 10 <sup>-6</sup>								

\*\* Tested by Internal Laboratory  
\*\*\* Approximate value  
† Sample dimension with 4 support points (L, W) 540x50mm; distance among the lower points 500mm, distance among the upper points 250mm  
‡ Values for a panel with a honeycomb core of Ø6 56kg/m³ (Ø 1/4")

1/2

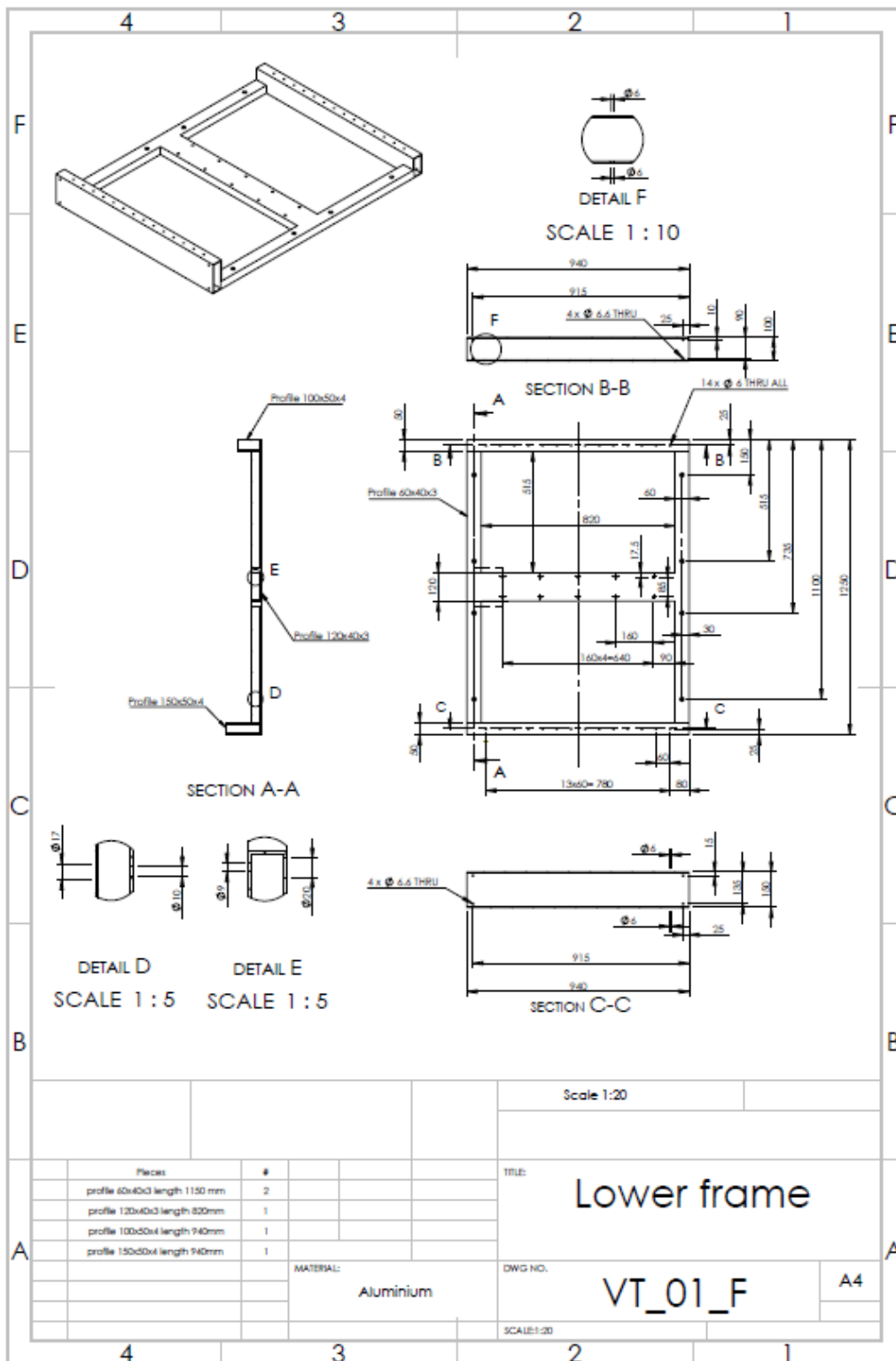


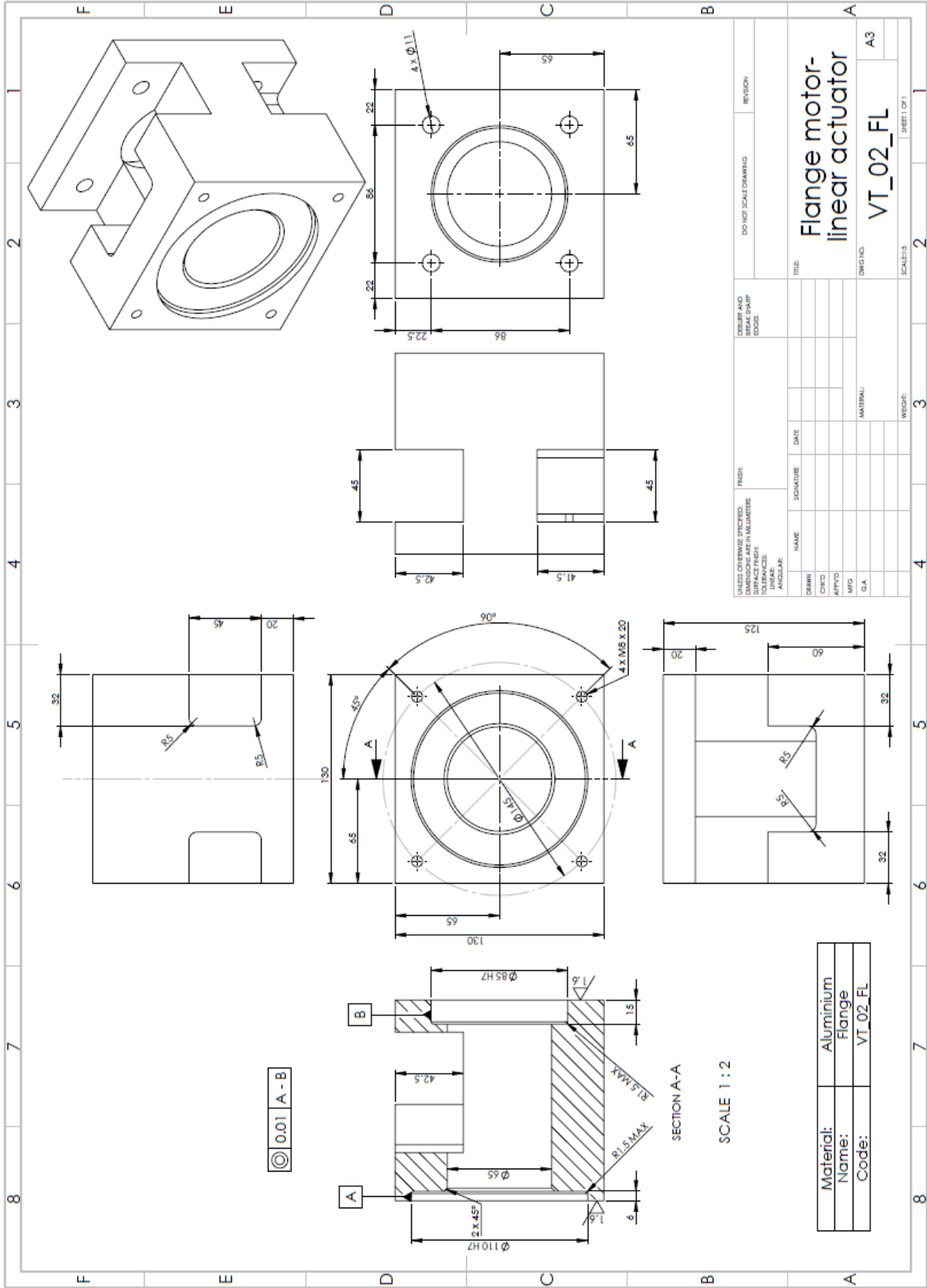
LIABILITY DISCLAIMER: The above data are to the best of our knowledge correct and are intended to give information about our products and their potential applications. No warranty is given or implied in respect of certain properties of the products or their suitability for a particular application. We reserve the right for technical changes without further notice. We guarantee impeccable product quality under our terms of sale.

Sandwich Panel Compoce® AL

Last Revised:03/20\_Rev.11

## [A.2] Drafts of custom parts





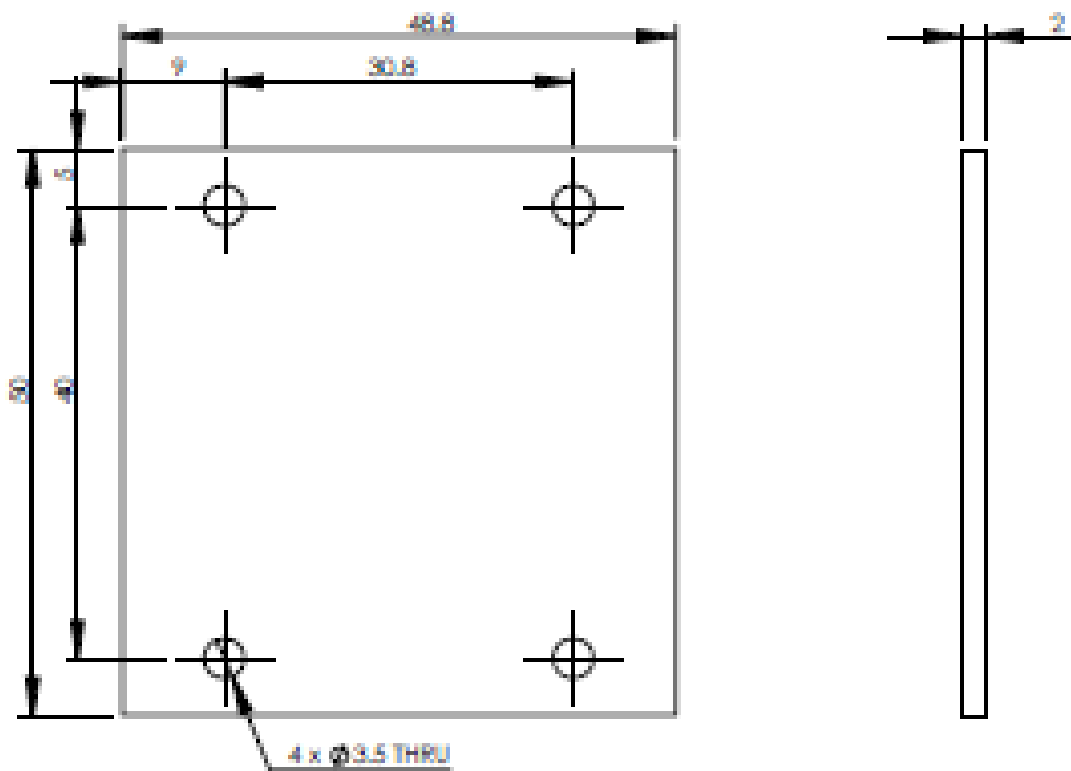
Ⓢ 0.01 | A - B

SECTION A-A

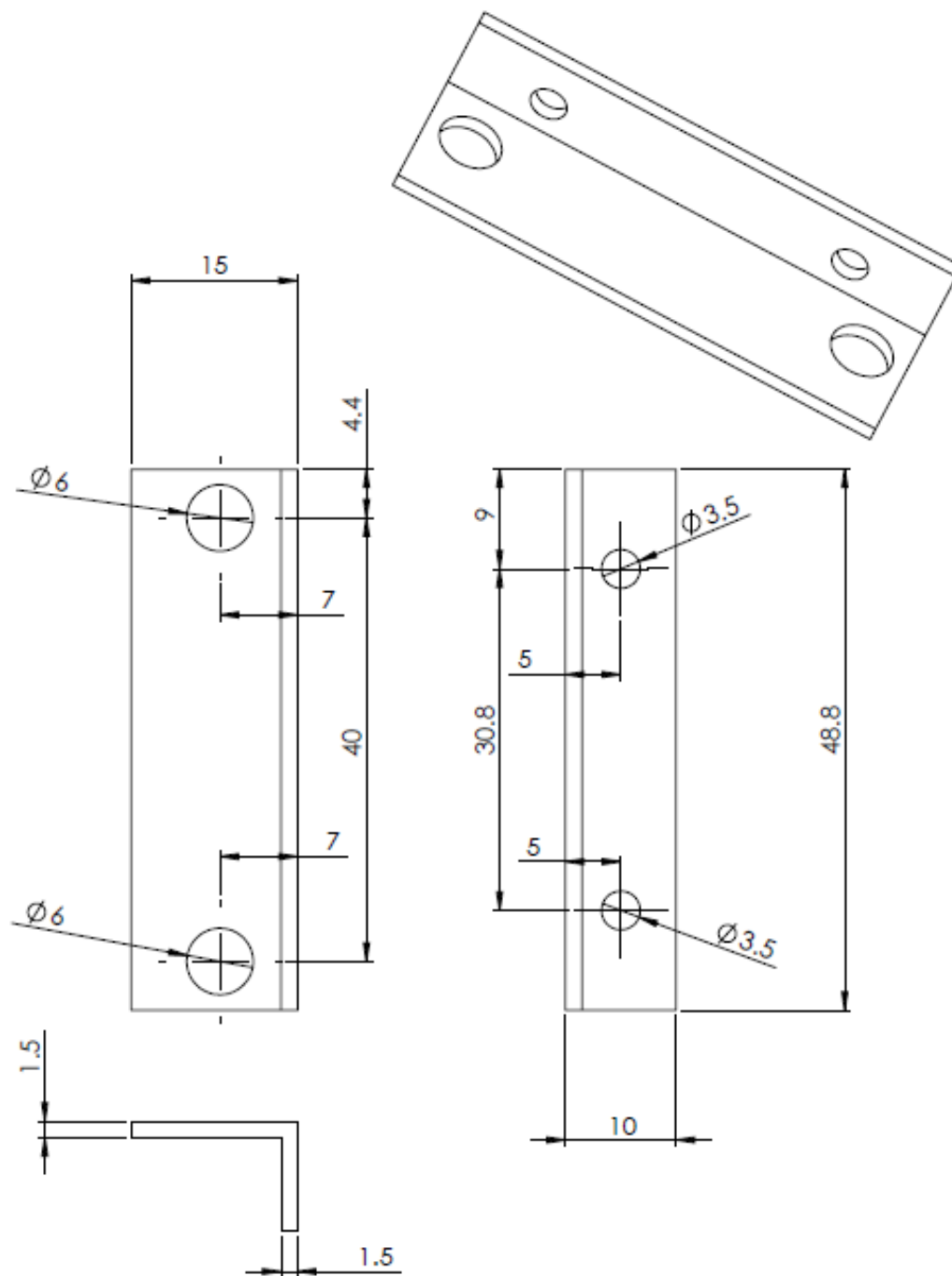
SCALE 1 : 2

Material:	Aluminium
Name:	Flange
Code:	VT_02_FL

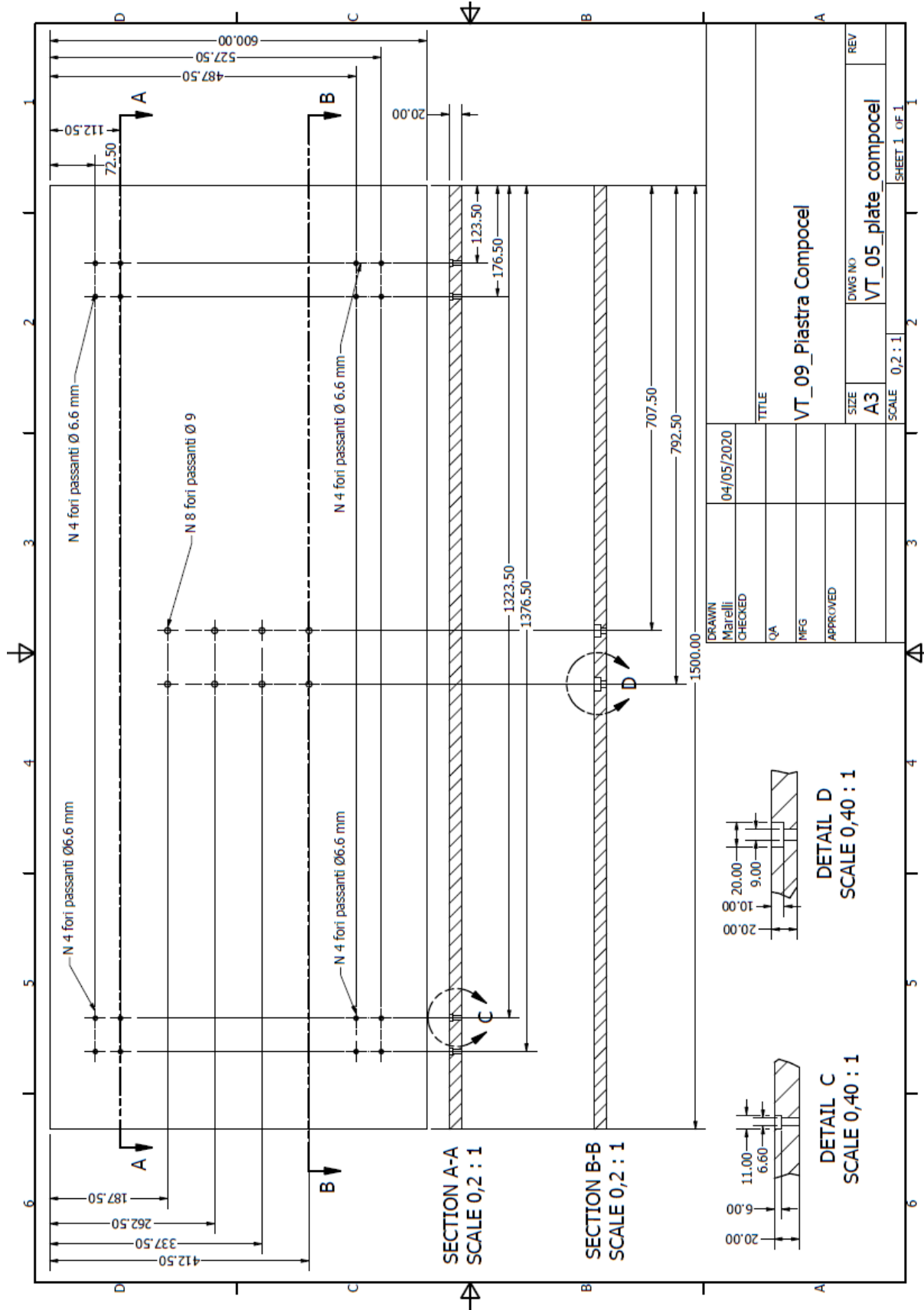
UNLESS OTHERWISE SPECIFIED: DIMENSIONS ARE IN MILLIMETERS SURFACE FINISH: TOLERANCES: ANGULAR:		FINISH: RADIUS: CHAMFER: EDGES:		DO NOT SCALE DRAWING		REVISION	
DATE:	SIGNATURE:	DATE:	SIGNATURE:	NAME:	DATE:	TITLE:	REVISION
DRAWN:	CHECKED:	APPROVED:	MFG:	Q.A.	MATERIAL:		
TITLE: <b>Flange motor-linear actuator</b>				DWG NO.: <b>VT_02_FL</b>			
SCALE: 1:2				SHEET 1 OF 1			



Material:	Aluminium
Name:	Vertical blade
Code:	VT_03_VB



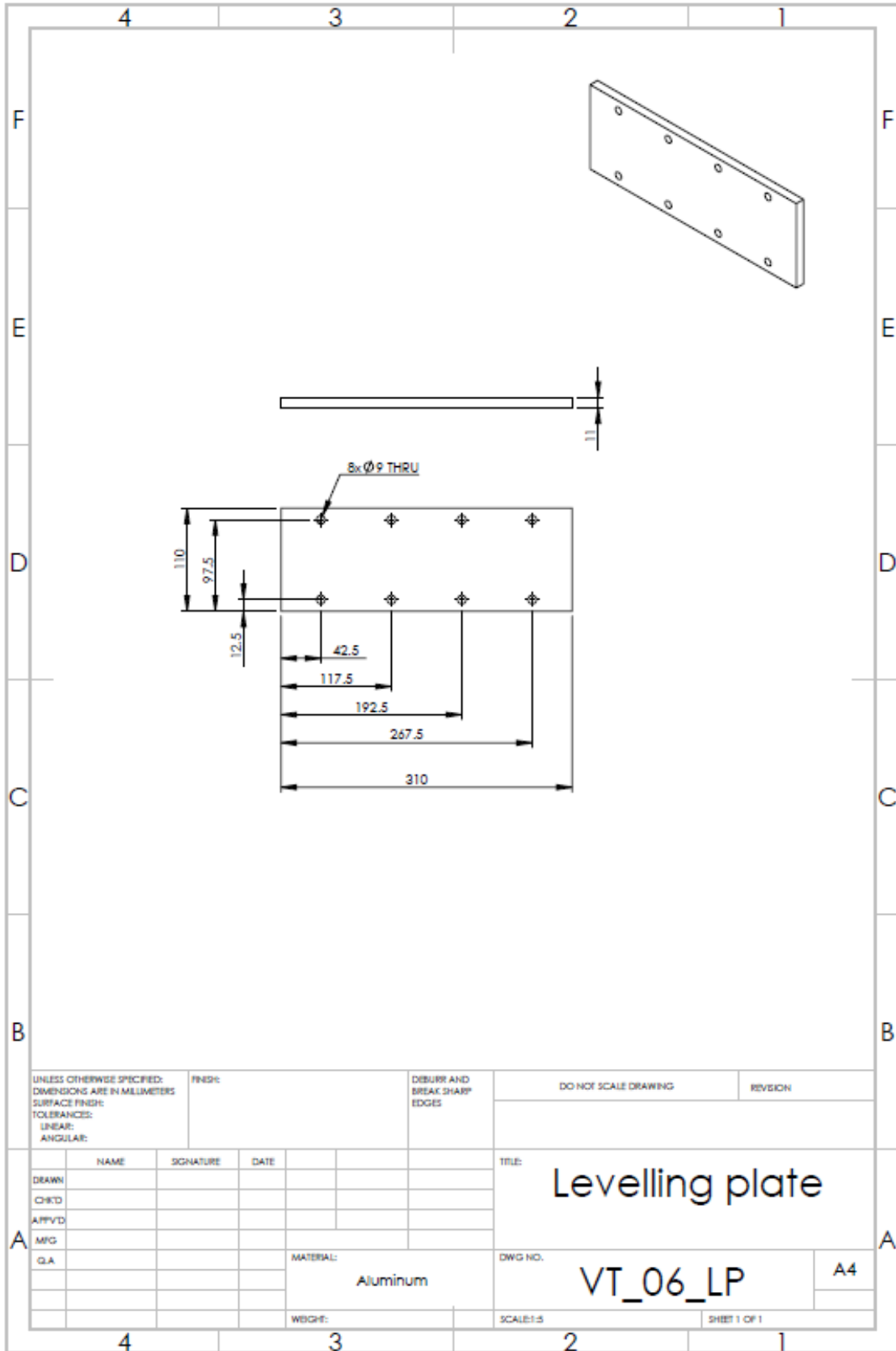
Material:	Aluminium
Name:	Blade fixer
Code:	VT_04_BF



DATE	04/05/2020
DRAWN	Maiselli
CHECKED	
Q/A	
MFG	
APPROVED	
TITLE	VT_09_Piastra Compoel
SIZE	A3
DWG NO	VT_05_plate_compoel
REV	
SCALE	0,2:1
SHEET	1 OF 1

SECTION A-A	SCALE 0,2 : 1
SECTION B-B	SCALE 0,2 : 1
DETAIL C	SCALE 0,40 : 1
DETAIL D	SCALE 0,40 : 1





UNLESS OTHERWISE SPECIFIED: DIMENSIONS ARE IN MILLIMETERS SURFACE FINISH: TOLERANCES: LINEAR: ANGULAR:			FINISH:		DEBURR AND BREAK SHARP EDGES		DO NOT SCALE DRAWING		REVISION		
DRAWN			SIGNATURE		DATE		TITLE: <b>Levelling plate</b>				
CHKD							DWG NO. <b>VT_06_LP</b>				
APPVD											
MFG							MATERIAL: <b>Aluminum</b>		SCALE: 1:5		SHEET 1 OF 1
QA							WEIGHT:		A4		

## [A.3] Matlab script

```
% Given a certain signal of vibration (velocity and
% acceleration)
% gives the possible combinations of motors and screws
% the results are a table with the different motors as rows and
% screws as columns (when it says true it means is a possible
% combination)
close all
clear all
clc

%% Input signal amplitude and frequency
t=linspace(0,10);
f=1.125;
Amp=0.1;      % assumed a sinusoidal signal with stroke +-0.1m and
              % freq 1.125 Hz (max acel 5 m/s^2 aprox)

% f=10;
% Amp=1.25e-3; % assumed a sinusoidal signal with stroke +-
              % 1.25mm and freq 10 Hz (max acel 5 m/s^2
              % aprox)

Vel=Amp*2*pi*f*cos(2*pi*f*t);
Acel=-Amp*(2*pi*f)^2*sin(2*pi*f*t);

vel_max=max(Vel); % Input Amp in meters and freq in Hz
acel_max=max(Acel);
acel_rms=rms(Acel);
vel_rms=rms(Vel);

AM=0.4;      % Apparent mass of human on the lateral direction
              % when applied a load also in lateral direction
M_t=AM*100+28+6.57; % maximum weight supported by treadmill(100
                  % Kg) times Aparent mass of human plus mass
                  % of treadmill (28 Kg) plus weight of
                  % Compocel aluminum plate (1500x600x20 mm^3)

%% Motors and actuators data from catalogues

T_M_N=[0.318 0.637 1.27 2.39 3.18 4.77 2.39 3.18 4.77 6.37 9.55
4.77 7.16 7.16 1.91 2.86 4.77 7.16 9.55 14.3 8.59 8.59 19.1
28.7]; % rated torque of motors [Nm]

T_M_max=[1.11 2.2 4.5 8.4 9.55 14.3 7.16 9.55 14.3 19.1 28.7
14.3 21.5 21.5 5.73 8.59 14.3 21.5 28.7 43 19.3 19.3 47.7 71.7];
% instantaneous peak torque [Nm]
```

```

J_M=[0.0968 0.2832 0.5052 2.0742 2.5542 2.5542 1.7542 2.5542
2.5542 2.8542 7.3122 6.5042 9.5042 7.99 2.8472 4.2472 6.5042
9.5042 12.7042 17.4122 9.5042 9.5042 45.1122 73.1122]*10^-4;
% rotor moment of inertia with brake [Kg*m^2]

w_M_max=[6000 6000 6000 6000 6000 6000 5000 5000 5000 5000 5000
3000 3000 3000 3000 3000 3000 3000 3000 3000 3000 2000 2000 2000
2000]*2*pi/60; % maximum speed of the motors [rad/s]

w_M_rated=[3000 3000 3000 3000 3000 3000 3000 3000 3000 3000
3000 2000 2000 2000 2000 2000 2000 2000 2000 2000 1000 1000 1000
1000]*2*pi/60; % rated speed of the motors [rad/s]

motor_names={'M10030T','M20030T','M40030T','M75030T','L1K030T','
L1K530T','L75030C','L1K030C','L1K530C','L2K030C','L3K030C','M1K0
20T','M1K520T','K1K520T','M40020C','M60020C','M1K020C','M1K520C'
,'M2K020C','M3K020C','M90010T','M90010C','M2K010C','M3K010C'};

l=0.6; % length of screw [m]

d=[12 12 12 12 16 16 16 16 16 16 20 20 25 20 20 25 12 12 16 16
20 20 20 20 25 25 25 32 32 32 20 20 32 32 32 20 20 25 25]/1000;
% diameter of screws [m]

p=[5 10 5 10 5 10 16 5 10 16 5 20 10 5 20 10 5 10 5 10 5 20 5 20
5 10 25 5 10 32 5 20 5 10 32 5 20 5 25]/1000/(2*pi);
% pitch of screw transmissions/(2pi) [m] (transmission ratio)

M_cart=[0.65 0.65 0.9 0.9 0.76 0.76 0.76 1.26 1.26 1.26 1.45
1.45 1.45 2.42 2.42 2.42 0.93 0.93 2.93 2.93 2.93 2.93 5.4 5.4
5.4 5.4 5.4 16.91 16.91 16.91 4 4 4 4 4 4 4 4];
% cart mass [Kg]

F_x=[4300 3600 4300 3600 12640 9900 9900 12640 9900 9900 14700
12250 16270 14700 12250 16270 6600 6600 12300 9600 14300 13300
14300 13300 15900 15700 14700 21600 31700 19500 14300 13300
21600 31700 19500 14300 13300 15900 14700];
% dynamic load capacity

V_cr=[[0.629 1.258 0.629 1.258 1.487 3.16 5.23 1.487 3.16 5.23
2.155 8.608 5.352 2.155 8.608 5.352]./(1-((1-0.3*1000*2)/2))^2
[0.65 1.3 1.63 3.25 2.13 8.42 2.13 8.42 2.76 5.52 13.48 3.58
7.03 22.5]./(646-((646-320)/2))^2 [2.13 8.42]./(660-((660-
200)/2))^2 [3.58 7.03 22.05]./(725-((725-200)/2))^2 [2.13 8.42
2.76 13.48]./(520-((520-200)/2))^2]*10^5;
% Velocity max due to critical velocity [m/s]

```

```

V_max=[0.56 1.11 0.56 1.11 0.42 0.83 1.33 0.42 0.83 1.33 0.33
1.33 0.53 0.33 1.33 0.53 0.5 1 0.5 1 0.5 2 0.5 2 0.5 1 2.5 0.4
0.8 2.5 0.5 2 0.4 0.8 2.5 0.5 2 0.5 2.5];
% maximum linear velocity ISO 7 [m/s]

screw_names={'TH901205SP2','TH901210SP2','TH901205SP4','TH901210
SP4','TH1101605SP2','TH1101610SP2','TH1101616SP2','TH1101605SP4'
,'TH1101610SP4','TH1101616SP4','TH1452005SP2','TH1452020SP2','TH
1452510SP2','TH1452005SP4','TH1452020SP4','TH1452510SP4','TT1001
205','TT1001210','TT1551605','TT1551610','TT1552005','TT1552020'
,'TT2252005','TT2252020','TT2252505','TT2252510','TT2252525','TT
3103205','TT3103210','TT3103232','TV802005','TV802020','TV110320
5','TV1103210','TV1103232','TV1402005','TV1402020','TV1402505','
TV1402525'};

rho_st= 7800; % density steel [kg/m^3]
J_T=rho_st*pi*d.^4*l/32; % moment of inertia of the screw
% [Kg*m^2]

J_L=M_t*(p/(pi*2)).^2; % moment of inertia of the load [Kq*m^2]
% since the load is linear

F_L_star_rms=M_t*acel_rms; % instead of torque we use a linear
% force

%% Calculation of alpha, beta and constraints
alpha=(T_M_N.^2)./J_M;
beta=2*((acel_rms*F_L_star_rms)+((M_t)*mean(Acel.^2)));

set(0,'DefaultLegendAutoUpdate','off')
for i=1:length(J_M)
    for j=1:length(p)
tau_min(i)=sqrt(J_M(i))*(sqrt(alpha(i) - beta +
4*acel_rms*F_L_star_rms)- sqrt(alpha(i)-beta))/(2*F_L_star_rms);

tau_max(i)=sqrt(J_M(i))*(sqrt(alpha(i) - beta +
4*acel_rms*F_L_star_rms)+ sqrt(alpha(i)-
beta))./(2*F_L_star_rms);

tau_kin(i)=vel_max/w_M_max(i);

tau_opt(i)=sqrt(J_M(i)*acel_rms/F_L_star_rms);

T_max=M_t*acel_max*p(j)+acel_max/p(j)*J_T(j)+acel_max*p(j)*M_car
t(j);

```

```

trans(i,j)=(p(j)>=tau_min(i) & p(j)>=tau_kin(i) &
p(j)<=tau_max(i) & T_M_max(i)>T_max & vel_max<V_max(j) &
vel_max<V_cr(j) & F_x(j)>(M_t+M_cart(j))*acel_max &
w_M_max(i)>vel_max/p(j) & w_M_rated(i)>vel_rms/p(j));
% Constraints the couple needs to satisfy

if trans(i,j)==true
mot_scr(i,j)=j;
end

end

plot(i,tau_min(i),'rv');
hold on
plot(i,tau_max(i),'b^');
plot(i,tau_opt(i),'go');
plot(i,tau_kin(i),'kp');
legend ('tau min','tau max','tau opt','tau kin')
xlabel('Motors')
ylabel('Pitch/(2\pi) [mm]')
end
for i=1:length(p)
plot(1:1:length(J_M),ones(1,length(J_M))*p(i))
end
T=array2table(trans,'VariableNames',screw_names,'RowNames',motor_names)
figure()
title('couple motor-screw');ylabel('screws');xlabel('motors')
for i=1:length(d)
motors=[1:1:length(J_M)];
hold on
plot(motors,mot_scr(:,i),'o')
grid on
end

```